



UNIVERSITY OF LEEDS

This is a repository copy of *Connectivity-based functional analysis of dopamine release in the striatum using diffusion-weighted MRI and positron emission tomography.*

White Rose Research Online URL for this paper:
<http://eprints.whiterose.ac.uk/88660/>

Version: Accepted Version

Article:

Tziortzi, AC, Haber, SN, Searle, GE et al. (9 more authors) (2014) Connectivity-based functional analysis of dopamine release in the striatum using diffusion-weighted MRI and positron emission tomography. *Cerebral Cortex*, 24 (5). 1165 - 1177. ISSN 1047-3211

<https://doi.org/10.1093/cercor/bhs397>

Reuse

Unless indicated otherwise, fulltext items are protected by copyright with all rights reserved. The copyright exception in section 29 of the Copyright, Designs and Patents Act 1988 allows the making of a single copy solely for the purpose of non-commercial research or private study within the limits of fair dealing. The publisher or other rights-holder may allow further reproduction and re-use of this version - refer to the White Rose Research Online record for this item. Where records identify the publisher as the copyright holder, users can verify any specific terms of use on the publisher's website.

Takedown

If you consider content in White Rose Research Online to be in breach of UK law, please notify us by emailing eprints@whiterose.ac.uk including the URL of the record and the reason for the withdrawal request.



eprints@whiterose.ac.uk
<https://eprints.whiterose.ac.uk/>



**Connectivity-based functional analysis of dopamine release
in the striatum using Diffusion Weighted MRI and Positron
Emission Tomography**

Journal:	<i>Cerebral Cortex</i>
Manuscript ID:	CerCor-2012-01046.R1
Manuscript Type:	Original Articles
Date Submitted by the Author:	n/a
Complete List of Authors:	Tziortzi, Andri; FMRIB Centre, University of Oxford, Clinical Neurosciences Haber, Suzanne; University of Rochester, Pharmacology and Physiology Searle, Graham; GlaxoSmithKline, Clinical Imaging Centre Tsoumpas, Charalampos; King's College London, Division of Imaging Sciences & Biomedical Engineering Long, Christopher; MIT, Sloan School of Management Shotbolt, Paul; Imperial College London, Department of Medicine Douaud, Gwenaelle; FMRIB Centre, University of Oxford, Clinical Neurosciences; Jbabdi, Saad; FMRIB Centre, University of Oxford, Clinical Neurosciences Behrens, Timothy; FMRIB Centre, University of Oxford, Clinical Neurosciences Rabiner, Eugenio; GlaxoSmithKline, Clinical Imaging Centre, Hammersmith Hospital, Imperial College London Jenkinson, Mark; University of Oxford, FMRIB Centre Gunn, Roger; GlaxoSmithKline, Clinical Imaging Centre, Hammersmith Hospital, Imperial College London; Imperial College London, Department of Medicine
Keywords:	DWI, Dopamine receptors, PET, Probabilistic Tractography, Striatum

1
2
3 Title: Connectivity-based functional analysis of dopamine release in the striatum using Diffusion Weighted MRI
4 and Positron Emission Tomography
5

6
7 Running title: Measurement of Striatal dopamine release
8

9
10 Author Names: Andri C. Tziortzi^{1,2}, Suzanne N. Haber³, Graham Searle², Charalampos Tsoumpas⁴, Christopher
11 Long², Paul Shotbolt^{2,5}, Gwenaelle Douaud¹, Saad Jbabdi¹, Timothy Behrens¹, Eugenio A. Rabiner^{2,5}, Mark
12 Jenkinson^{1,*}, Roger N. Gunn^{2,5,6,*}
13
14

15
16 Affiliations: 1. FMRIB centre, Nuffield Department of Clinical Neurosciences, University of Oxford, UK, 2.
17 GlaxoSmithKline Clinical Imaging Centre, Hammersmith Hospital, London, UK , 3. University of Rochester,
18 School of Medicine and Dentistry, Rochester, USA, 4. Division of Imaging Sciences & Biomedical Engineering,
19 King's College London, UK, 5. Department of Medicine, Imperial College London, UK, 6. Department of
20 Engineering Science, University of Oxford, UK, * Authors contributed equally.
21
22
23
24
25
26

27
28 Corresponding author: Professor Roger Gunn. Imanova Limited, Burlington Danes Building, Hammersmith
29 Hospital, Du Cane Road, London W12 0NN, UK. Tel: +44-2080086000, Email: Roger.Gunn@imanova.co.uk
30
31

32
33
34 Keywords: DWI, Dopamine receptors, PET, Probabilistic Tractography, Striatum.
35
36
37
38
39
40
41
42
43
44
45
46
47
48
49
50
51
52
53
54
55
56
57
58
59
60

Abstract

The striatum acts in conjunction with the cortex to control and execute functions that are impaired by abnormal dopamine neurotransmission in disorders such as Parkinson's and schizophrenia. To date, in-vivo quantification of striatal dopamine has been restricted to structural-based striatal subdivisions. Here, we present a multi-modal imaging approach that quantifies the endogenous dopamine release following administration of d-amphetamine in the functional subdivisions of the striatum of healthy humans with [^{11}C]PHNO and [^{11}C]Raclopride PET ligands. Using connectivity-based parcellation, we subdivided the striatum into functional sub-regions based on striato-cortical anatomical connectivity information derived from diffusion MRI and probabilistic tractography. Our parcellation showed that the functional organisation of the striatum was spatially coherent across individuals, congruent with primate data and previous diffusion MRI studies, with distinctive and overlapping networks. D-amphetamine induced the highest dopamine release in the limbic followed by the sensory, motor and executive areas. The data suggest that the relative regional proportions of D2-like receptors are unlikely to be responsible for this regional dopamine release pattern. Notably, the homogeneity of dopamine release was significantly higher within the connectivity-based functional subdivisions in comparison with the structural subdivisions. These results support an association between local levels of dopamine release and cortical connectivity fingerprints.

Introduction

Over the last two decades the dopaminergic system has been studied extensively with Positron Emission Tomography (PET) (Egerton et al. 2009; Laruelle 2012). These imaging studies have investigated the density and distribution of dopamine receptors, dopamine synthesis and dopamine release into the extracellular space following a range of pharmacological or behavioural stimuli in healthy and diseased populations (Kegeles et al. 2010; Mizrahi et al. 2011; Banerjee and Prante 2012; Boileau et al. 2012; Mizrahi et al. 2012; Suridjan et al. 2012). The basal ganglia (BG), and in particular the striatum, has been the focus due to an abundance of dopamine receptors and involvement in dopamine related diseases such as Parkinson's and schizophrenia. The striatum acts in conjunction with the cortex to control and execute functions and it has been divided into closed cortical–BG–thalamo–cortical loops (limbic, executive, motor, sensory) with each structure maintaining the functional characteristics of the projective region (Parent and Hazrati 1995; Haber 2003; Haber et al. 2006). The striatum is a heterogeneous structure, which consists of three cytoarchitectonically-undifferentiated areas: the caudate, putamen and nucleus accumbens. While the caudate and putamen are anatomically separate nuclei, the nucleus accumbens has been defined simply as the ventral striatal region abutting the septum.

Autoradiography and molecular PET imaging studies have shown that the receptors and release of dopamine are not always uniformly distributed or released within the traditional structural striatal subdivisions (Staley and Mash 1996; Gurevich and Joyce 1999; Martinez et al. 2003). Nonetheless, to date the regional quantification of dopamine release within the striatum has been based on these traditional subdivisions (Drevets et al. 1999; Martinez *et al.* 2003; Narendran et al. 2004; Shotbolt et al. 2011). More recently functional subdivisions of the primate and human striatum have been introduced based on the distribution of its cortical inputs (Selemon and Goldman-Rakic 1985; Parent and Hazrati 1995; Haber 2003; Lehericy et al. 2004; Croxson et al. 2005; Leh et al. 2007; Draganski et al. 2008; Cohen et al. 2009; Bohanna et al. 2011; Tziortzi, Searle, Tsoumpas, et al. 2011). These studies demonstrate the existence of individual and overlapping cortical-striatal networks and reveal the topographical organisation of these networks. Moreover it has been shown (Haber *et al.* 2006) that the limbic portion of the striatum occupies a large rostral striatal region that extends beyond the boundaries of the nucleus accumbens.

1
2
3 The aim of this study is to quantify amphetamine-induced dopamine release in the connectivity-based
4 functional subdivisions of the human striatum. Quantification of dopamine in the functional territories may
5 provide new insights about dopamine function, help understand the neurochemical organisation and
6 potentially help the development of novel therapeutic compounds and comprehension of dopamine related
7 neurological disorders. The first part of this paper determines, in individual subjects, the cortical-striatal
8 projections to functionally parcellate the striatum using diffusion-weighted MRI and probabilistic tractography
9 (Behrens, Johansen-Berg, et al. 2003). The second part applies these functional subdivisions to PET
10 neurotransmission data to quantify regional dopamine release following the administration of d-
11 amphetamine. To examine whether dopamine release has a functional or a structural specificity dopamine is
12 also measured in the structural subdivisions of the striatum in the same subjects and the measurements are
13 compared. PET data from two D2/D3 dopamine ligands were investigated: the agonist [¹¹C]PHNO, which has a
14 preferential affinity for the D3 receptor (Gallezot et al. 2012) and the antagonist [¹¹C]Raclopride, which has
15 equal affinity for the D2/D3 receptors. This enables testing of the robustness of the findings across two PET
16 radioligands and investigation of whether the regional detection of dopamine release depends upon the
17 relative distribution of the D2/D3 receptors and the ligands preferential affinities.
18
19
20
21
22
23
24
25
26
27
28
29
30
31
32
33
34
35
36
37
38
39
40
41
42
43
44
45
46
47
48
49
50
51
52
53
54
55
56
57
58
59
60

Material and Methods

In the first part of the paper, probabilistic tractography is used to parcellate the human striatum into connectivity-based functional regions of interest (ROIs) based on the striato-cortical connections. To obtain the connectivity-based functional regions in each subject a two-step procedure was applied: a) projections from the four brain lobes (frontal, parietal, occipital, temporal) to the striatum were estimated and the striatal areas associated with each lobe were established; b) The frontal lobe was subdivided into four anatomical ROIs, each associated with a particular functional specialisation (limbic, executive, rostral motor and caudal motor), and projections between these anatomical ROIs and the striatal area associated with the frontal lobe was estimated (figure 1B, methods overview).

In the second part of the paper, these functional subdivisions were used in conjunction with the [¹¹C]PHNO and [¹¹C]Raclopride PET neurotransmission data in order to quantify regional specific dopamine release following a d-amphetamine challenge. For comparison, the dopamine release was also quantified within structural subdivisions (Martinez *et al.* 2003; Tziortzi, Searle, Tzimopoulou, et al. 2011).

Subjects

The study was conducted at the GlaxoSmithKline Clinical Imaging Centre, Hammersmith Hospital, London and was approved by Essex 1 Research Ethics Committee and the Administration of Radioactive Substances Advisory Committee (ARSAC) and subjects provided written informed consent. The data analysed and presented here were obtained from a cohort of subjects described previously (Shotbolt *et al.* 2011). In short, twelve healthy male volunteers were recruited aged between 25 and 55 years, free from clinically significant illness or disease as determined by their medical history and standard laboratory tests. Each subject underwent a series of MRI and PET scans including a T1-weighted and diffusion-weighted MRI. Nine subjects completed four PET scans, two with [¹¹C]PHNO and two with [¹¹C]Raclopride in a counterbalanced order. A further three subjects received only two [¹¹C]PHNO scans as two of them dropped out of the study, and the third was withdrawn because of an incidental finding. For each ligand, subjects initially received a baseline scan and then d-amphetamine was administered orally (0.3mg/kg) on an empty stomach three hours prior to the start of the challenge scan.

Image acquisition and pre-processing

1
2
3 **MRI.** High-resolution T1-weighted and diffusion-weighted images were acquired with a 32-channel head coil
4 on a Siemens Tim Trio, 3T MRI scanner (Siemens Healthcare, Erlangen, Germany). An isotropic T1-weighted (1
5 mm³) image was acquired with a magnetisation-prepared rapid gradient echo (MPRAGE) sequence (TR = 3000
6 ms, TE = 3.66 ms, flip angle of 9°, TI = 1100 ms, matrix = 256 x 192. A parallel imaging factor of 2 was applied to
7 enable an acquisition time of 321 s).
8
9

10
11
12 Diffusion-weighted data were acquired using echo planar imaging (EPI) (TR = 9000 ms, TE = 86 ms, flip angle of
13 90° and voxel size of 1.875 x 1.875 x 1.9 mm³). The diffusion weighting was isotropically distributed along 30
14 directions (b-value=1000 s/mm²) and a non-diffusion-weighted image (B0) was acquired at the beginning of
15 each scan. EPI acquisitions are prone to geometric distortions which can lead to errors in tractography. To
16 minimise this, two image sets were acquired with the phase encoded direction reversed – ‘blip-up’ and ‘blip-
17 down’ (Chang and Fitzpatrick 1992) – resulting in images with geometric distortions of equal magnitude but in
18 the opposite direction allowing for the calculation of a corrected image (Andersson et al. 2003). Before
19 correcting geometric distortions each image set – ‘blip-up’ and ‘blip-down’ – was corrected for motion and
20 eddy-current related distortions. Diffusion data analysis was performed with the FSL tools (FMRIB Centre
21 software library, Oxford University; <http://www.fmrib.ox.ac.uk/fsl/>).
22
23
24
25
26
27
28
29
30
31
32
33
34

35 **PET.** All subjects were scanned on a Siemens Biograph HiRez XVI PET scanner (Siemens Healthcare, Erlangen,
36 Germany), under baseline conditions (no challenge) and three hours following the oral administration of 0.3
37 mg/kg of d-amphetamine. For each scan, subjects were injected with a single intravenous bolus of [¹¹C]PHNO
38 or [¹¹C]Raclopride and dynamic emission data were acquired continuously for 90 minutes. Six of the subjects
39 had their two [¹¹C]PHNO scans on the same day with at least five hours between [¹¹C]PHNO injections,
40 whereas the other six subjects had their two scans on separate days. [¹¹C]Raclopride scans were acquired on
41 the same day. The dynamic images were reconstructed, into 26 frames (8x15 s, 3x1 min, 5x2 min, 5x5 min and
42 5x10 min), using a filtered back projection algorithm (direct inversion Fourier transform; DIFT) with a 128
43 matrix, zoom of 2.6 producing images with isotropic voxel size of 2x2x2 mm³, and a transaxial Gaussian filter of
44 5mm. A low dose CT scan (effective dose 0.2mSv) was acquired for attenuation and scatter correction. The
45 dynamic PET data were corrected for motion via frame-to-frame image registration and aligned with the
46
47
48
49
50
51
52
53
54
55
56
57
58
59
60

1
2
3 structural T1 MRI image using SPM5b (Wellcome Trust Centre for Neuroimaging,
4 <http://www.fil.ion.ucl.ac.uk/spm>) with a mutual information cost function.
5
6
7

8 9 **Connectivity-based functional subdivision of the striatum**

10
11 **Probabilistic Tractography.** The FMRIB's diffusion toolbox (<http://www.fmrib.ox.ac.uk/fsl/fdt>) was used to
12 perform probabilistic tractography with a partial volume model (Behrens, Woolrich, et al. 2003) allowing for up
13 to two fiber directions in each voxel (Behrens et al. 2007). Five thousand sample tracts were generated from
14 each voxel in the seed mask (striatum). Tractography was performed in the subjects' continuous space and
15 the results were output in the Montreal Neurological Institute (MNI) space by providing transformation
16 parameters estimated via a two-step procedure as follows: a) the fractional anisotropy image was registered
17 to each subject's high resolution T1-weighted image using FLIRT (Jenkinson et al. 2002) with 6 degrees of
18 freedom and a mutual information cost function; b) The T1-weighted image was non-linearly registered to the
19 1x1x1 mm³ nonlinear MNI template with FNIRT. The transformation parameters obtained from these two
20 steps were concatenated to yield the mapping from the diffusion-weighted image (DWI) to MNI space.
21
22
23
24
25
26
27
28
29
30
31

32 **Functional subdivision - phase I.** The projections from the striatum to the frontal, parietal, occipital and
33 temporal cortical areas were estimated. For each striatal voxel we calculated the probability of connection to
34 each area as the proportion of the total number of samples, which originate from this voxel and reach any
35 cortical area. Then, the striatum was segmented by assigning each voxel to the lobe with which it had the
36 highest connection probability (Johansen-Berg et al. 2005). After this 'hard' segmentation, the areas in
37 striatum that associate with each lobe were established.
38
39
40
41
42
43
44

45 **Functional subdivision - phase II.** The striatal area found in phase I to be associated with the frontal lobe, is
46 further subdivided into the following functional regions: a) limbic, involved in emotions, reward and
47 motivation; b) executive, linked to executive processes such as perception, memory, reasoning and judgment;
48 c) rostral-motor, involved in the planning and control of movements; and d) caudal-motor, involved with the
49 execution of movements. Four frontal lobe anatomical subdivisions (described below), each associated with
50 the aforementioned functions, were used to estimate the connections with the striatal area associated with
51
52
53
54
55
56
57
58
59
60

1
2
3 the frontal lobe. Note that the prefrontal ROIs were not derived from functional MRI experiments but make
4 use of the known areas of specific brain function, as determined from the human and primate literature.
5
6

7
8 For each subject and hemisphere seven connection maps were derived, one for each cortical target (limbic,
9 executive, rostral-motor, caudal-motor, parietal, occipital and temporal). Since individual and overlapping
10 cortical-striatal networks exist, striatal voxels are either connected exclusively to a cortical target or show
11 connectivity to multiple cortical regions. To accommodate this finding we process the connectivity maps in two
12 different ways:
13
14
15
16

17
18 a) For each subject, exclusive connectivity-based functional ROIs (**CB**) were created following the procedures
19 described by Johansen-Berg and colleagues (2005). In brief, for each striatal voxel the probability of connection
20 to each cortical target was calculated as a proportion of the total number of samples from that voxel that
21 reach any cortical area; Next, each voxel was assigned to the cortical target with the highest connection
22 probability.
23
24
25
26
27

28
29 b) Each subject's connectivity maps were thresholded at 5% (Croxson *et al.* 2005) of the maximum connectivity
30 value to exclude noise and voxels with low connectivity values. This allowed functional subdivisions to have a
31 certain degree of overlap (overlapping networks). The functional areas obtained with this method will be
32 abbreviated as **CBo**.
33
34
35
36

37
38 **Regions of interest preparation.** The complete striatum outline was manually defined on the subject's T1-
39 weighted image and the cortical lobes were obtained from the CICAtlas, (Tziortzi, Searle, Tzimopoulou, *et al.*
40 2011) a modification of the Harvard-Oxford atlas. In addition, the frontal lobe was subdivided into 4
41 anatomical regions, based on known anatomical classification of function (figure 1A). Details of the four frontal
42 lobe subdivisions are as follows:
43
44
45
46
47

48
49 Limbic target: The structures comprising the limbic anatomical ROI are the anterior orbital gyrus, posterior
50 orbital gyrus, medial orbital gyrus, gyrus rectus (Chiavaras and Petrides 2000), and subcallosal gyrus – ventral
51 anterior cingulate (parolfactory area – area 25). The lateral orbital gyrus was excluded since several studies
52 report that it has a different connectivity pattern and function from the medial orbital cortex (Kringelbach and
53 Rolls 2004; Wallis 2007).
54
55
56
57
58
59
60

1
2
3 Executive target: The functional map proposed by Petrides (2005) was adopted to delineate areas 9, 9/46 and
4 area 10 of dorsolateral prefrontal cortex which constituted the executive ROI. Anatomically, the ROI consisted
5 of the rostral superior and middle frontal gyri and the dorsal prefrontal cortex (3 mm dorsal the mid-sagittal
6 most anterior and dorsal tip of gyrus rectus, where area 10 is situated).
7
8
9

10
11 Rostral-motor target: The caudal portions of lateral and medial superior gyrus, and the caudal middle and
12 inferior frontal gyri were included in the rostral-motor target. These anatomical regions correspond
13 functionally to rostral area 6, supplementary motor area (SMA), pre-SMA and the frontal eye field region.
14
15
16

17
18 Caudal-motor target: Includes the pre-central gyrus, which corresponds functionally to the primary motor
19 cortex (area 4) and the caudal premotor area (caudal area 6). The paracentral lobule was excluded from the
20 target.
21
22
23

24
25 To tailor the cortical ROIs to the subjects' individual anatomy, the subjects' segmented grey matter (GM) and
26 fractional anisotropy (FA) images, both normalised to the MNI template, were employed to mask the ROIs. The
27 lower threshold for the GM mask was set at 0.25 and the FA mask upper threshold was set at 0.40.
28
29
30

31 **Structural subdivision and structural-based functional subdivision of the striatum**

32
33 A structural based method that uses anatomical landmarks to subdivide the striatum, based on a previously
34 described method (Tziortzi, Searle, Tzimopoulou, *et al.* 2011), was also employed for comparison with the
35 connectivity approach presented here. Several studies have shown that there is not a definitive anatomical,
36 histological or histochemical distinction between nucleus accumbens, caudate and putamen. Therefore
37 structural based methods (Drevets *et al.* 1999; Mawlawi *et al.* 2001; Martinez *et al.* 2003) use arbitrary
38 anatomical landmarks in an attempt to subdivide the striatum: a) the striatum is subdivided into caudate (CD),
39 putamen (PU) and ventral striatum (VST). All the ROIs are defined on each subject's T1-weighted image
40 following the guidelines detailed in Tziortzi *et al.* (2011). This subdivision will be referred to as structural-based
41 ROIs (**SB**); b) the delineated PU is subdivided into pre- and post-commissural as described by Martinez *et al.*
42 (2003). This technique was proposed in an attempt to structurally approach the functional organisation of the
43 striatum. Specifically, the VST is classified as limbic striatum, the post-commissural putamen as sensorimotor
44 and the pre-commissural putamen with caudate as executive. These subdivisions will be referred to as
45 structural-based functional ROIs (**SBf**).
46
47
48
49
50
51
52
53
54
55
56
57
58
59
60

Quantification of regional dopamine release

The basis function implementation of the simplified reference tissue model (SRTM) (Lammertsma and Hume 1996; Gunn et al. 1997) was applied to the dynamic [^{11}C]PHNO and [^{11}C]Raclopride PET data. Using the cerebellum as a reference region, we derived parametric images of the non-displaceable binding potential (BP_{ND}), which is proportional to the receptor availability. Each subject's pre- and post-d-amphetamine parametric images were co-registered using FLIRT (Jenkinson *et al.* 2002) and then transformed into MNI space using the transformation parameters derived from non-linearly registering the subject's T1-weighted image to the $1 \times 1 \times 1 \text{ mm}^3$ nonlinear MNI template with FNIRT. Subsequently the **CB**, **CBo**, **SB** and **SBf** subdivisions of the striatum were applied to the [^{11}C]PHNO and [^{11}C]Raclopride BP_{ND} parametric images to calculate the regional estimates of BP_{ND} . The fractional change between baseline and post-d-amphetamine conditions then provides an index of the synaptic dopamine release as:

$$\Delta \text{BP}_{\text{ND}} = 100 \left(\frac{\text{BP}_{\text{ND}}^{\text{Base}} - \text{BP}_{\text{ND}}^{\text{Amph}}}{\text{BP}_{\text{ND}}^{\text{Base}}} \right) \% \quad (2)$$

where $\text{BP}_{\text{ND}}^{\text{Base}}$ is the BP_{ND} in the baseline condition and $\text{BP}_{\text{ND}}^{\text{Amph}}$ is the BP_{ND} following the administration of d-amphetamine (Laruelle 2000). The coefficient of variation (%COV) for the dopamine release was calculated to provide an index of homogeneity of dopamine release within each subdivision.

Results

Connectivity-based functional subdivision of the striatum

Projections from cortical lobes - phase I. While all cortical lobes project to the striatum, the areas that each lobe's efferent projections occupy are not equally represented. After hard segmentation of the striatum across subjects, the frontal lobe input dominates with 82 ± 7 % of the total striatal volume (frontal lobe grey matter volume: 248 ± 14 cm³), followed by the parietal lobe with 11 ± 5 % (parietal lobe grey matter volume: 116 ± 7 cm³), the temporal lobe with 5 ± 5 % (temporal lobe grey matter volume: 114 ± 3 cm³) and the occipital lobe with 2 ± 1 % (occipital lobe grey matter volume: 85 ± 3 cm³). The cortical projections were estimated for each subject and the group average inputs in the MNI space are shown in figure 2A.

The frontal lobe input occupies almost the entire caudate and pre-commissural putamen extending up to the post-commissural putamen. The parietal lobe, the second biggest cortical input, projects primarily to the post-commissural caudate and putamen with scattered projections observed in the pre-commissural caudate. In contrast to the projections from the frontal and parietal lobes, the projections from the occipital and temporal lobes are more confined (figure 2A-B). Small-interspersed projections from the temporal lobe were found in the pre-commissural caudate, nucleus accumbens and in the ventral post-commissural putamen whilst occipital projections were limited to the ventral post-commissural putamen. The projections of each lobe occupy distinctive striatal areas with a significant degree of overlap observed between frontal and parietal lobes in the post-commissural putamen and some overlap between frontal and temporal lobes in the nucleus accumbens and pre-commissural regions. The large number of frontal lobe projections into the striatum confirms that these two regions interact extensively to coordinate and execute function.

Projections from frontal lobe subdivisions - phase II. Distinct, overlapping and bilaterally symmetric projections from the four anatomical subdivisions of the frontal lobe (limbic, executive, rostral-motor and caudal-motor) were derived (figure 3A) and shown to be similar to those obtained from non-human primate tracing studies (Haber *et al.* 2006; Calzavara *et al.* 2007) and confirmatory of previous human DWI studies (Lehéricy *et al.* 2004; Draganski *et al.* 2008). The limbic striatum occupies the nucleus accumbens and ventral pre-commissural caudate and putamen. Of particular interest are the small patches of limbic projections

1
2
3 observed in the ventral post-commissural putamen, an area where projections from the temporal lobe and
4 amygdala can also be found. For pre-commissural striatum, the executive projections reside in the central and
5 dorsal striatum as opposed to the post-commissural striatum where they occupy the central and ventral zones.
6
7 *The rostral-motor target, projects to an elongated area that occupies the dorsal tiers of putamen and caudate.*
8
9 *In contrast, the caudal-motor projections are confined to the post-commissural putamen with only a few low*
10 *probability connections in the anterior dorsal caudate. In post-commissural putamen caudal-motor projections*
11 *occupy, in addition to dorsal areas, more central areas and its projections extend further caudal in comparison*
12 *to the rostral-motor occupied area. Figures 3B and 4A show the subdivisions with the **CB** method in four*
13 *representative subjects and the group averaged **CB** subdivisions respectively. The subdivisions are symmetrical*
14 *and spatially coherent across individuals. The group average subdivisions were defined using the methods*
15 *described in Johansen-Berg et al (2005).*
16
17
18
19
20
21
22
23

24
25 The volume and percentage contribution to the total striatal volume of the cortical projections as defined with
26 **CBo** and **CB** methods are shown in Table I with the projections from the executive target occupying the
27 greatest area. Temporal and occipital lobes occupy with **CBo** method 13.71% and 5.91% of the total striatal
28 volume respectively while with the **CB** method they occupy only 5% and 2%. However, the connection
29 probabilities from these lobes are low and following 'hard' segmentation these areas were small and not
30 spatially consistent across individuals and therefore are not reported.
31
32
33
34
35
36
37

38 To arithmetically assess the inter-subject spatial consistency of the **CB** and **CBo**, we estimated the DICE
39 coefficient i.e. the volume overlap of striatal subdivisions across subjects (detailed results is supplementary
40 material). The DICE values obtained for the limbic, executive and parietal striatum were high and satisfactory
41 for the smaller rostral-motor and caudal-motor regions. For comparison, connectivity-based functional ROIs
42 have been estimated with a threshold of 1% and 10% and the volumes can be seen in Table III in supplemental
43 material. Figure 6 (supplemental material) illustrates the impact of different thresholds on the topography and
44 size of the cortical projections.
45
46
47
48
49
50
51

52 **Frontal lobe overlapping projections.** Tracts from the frontal lobe led to overlapping pathways (figure 4B) and
53 were categorised as a) limbic - executive, b) executive – rostral-motor, c) executive – caudal-motor and d)
54 rostral-motor – caudal-motor. A threshold of 50 samples was applied to the projections and subsequently the
55
56
57
58
59
60

1
2
3 overlapping areas were determined. The limbic-executive overlap occupies the ventral medial area of the pre-
4 commissural caudate and the posterior and ventral post-commissural putamen. The location of this overlap
5 agrees with that of non-human primates as described by Haber and colleagues (2006). The executive – rostral-
6 motor overlap is the most extensive and resides in the dorsal pre-commissural striatum and post-commissural
7 putamen. Even though it is spatially consistent with the overlaps described in primates (Calzavara *et al.* 2007),
8 in our study appears to extend further in humans. The executive – caudal-motor overlap is found only in the
9 post-commissural striatum and specifically in the dorsal caudate and dorsal and central lateral putamen.
10 Finally, the rostral-motor – caudal-motor overlap is found in the post-commissural lateral putamen. In order to
11 examine the sensitivity of these finding to the arbitrary choice of threshold, we applied increasing levels of
12 threshold (1%, 5% and 10%) to the tractography results for each striatal projection. Although the occupied
13 volume of the overlapping areas changed substantially from the threshold of 1% to that of 10% the
14 aforementioned overlaps were preserved. This evidence and the fact that the existence and location of these
15 overlaps have been confirmed by tracing studies, supports their use to report dopamine release in the
16 corresponding areas.
17
18
19
20
21
22
23
24
25
26
27
28
29
30

31 **Release of dopamine in the striatal subdivisions**

32
33
34 Dopamine release in the structural and connectivity-based functional subdivisions post d-amphetamine was
35 inferred from the percentage change in [¹¹C]PHNO and [¹¹C]Raclopride BP_{ND}. The dopamine release and the
36 coefficient of variation (%COV) for the dopamine release, an index of homogeneity of dopamine release within
37 a region, were measured for the connectivity based (**CB**, **CB_o**) and structural based (**SB**, **SB_f**) subdivisions (table
38 II and figure 5).
39
40
41
42
43
44

45 For the connectivity-based methods a consistent pattern of dopamine release was found for both the two
46 ligands. Specifically, the highest dopamine release was measured in the limbic area followed by the parietal,
47 the caudal-motor and rostral-motor areas. The lowest dopamine release was measured in the executive
48 region. For each connectivity-based subdivision and for each ligand an analysis of variance (ANOVA) was
49 performed to assess whether the means of dopamine release, estimated with each method (**CB**, **CB_o**), were
50 different. The results demonstrate that the difference in dopamine release across methods is not significant.
51
52
53
54
55
56 The Shapiro-Wilk test (Shapiro and Wilk 1965) was applied to test the normality of the distributions.
57
58
59
60

1
2
3 In addition, ANOVA was implemented to assess if dopamine is differentially released in the striatal functional
4 subdivisions. For [¹¹C]PHNO data dopamine was differentially released in the striatal functional subdivisions for
5 both methods (p-values: **CB** = 0.002, **CBo** = 0.004). Multiple comparison tests with Bonferroni correction was
6 performed, to determine which pairs of functional areas exhibit significant difference in dopamine release.
7 Both methods, showed a significant difference between limbic – executive and between limbic – rostral-motor
8 areas. For [¹¹C]Raclopride, ANOVA shows that dopamine is differentially released in the **CBo** subdivisions (p =
9 0.01) whilst the **CB** subdivisions approached significance (p=0.09). For [¹¹C]Raclopride only the limbic –
10 executive pair defined with the **CBo** exhibited a significant difference in dopamine release whereas for the **CB**
11 method differences between limbic- executive areas did not survive corrections for multiple comparisons.
12
13
14
15
16
17
18
19

20
21 In the **SBf** subdivisions the highest dopamine release was in the limbic region (VST) ([¹¹C]PHNO = 21.2 ± 6.93 %, [¹¹C]Raclopride = 14.1 ± 6.38 %) followed by the sensorimotor (post-commissural putamen) ([¹¹C]PHNO = 16.8 ± 4.17 %, [¹¹C]Raclopride = 13.1 ± 6.82 %) and executive regions (caudate and pre-commissural putamen) ([¹¹C]PHNO = 13.4 ± 5.68 %, [¹¹C]Raclopride = 8.62 ± 5.09 %). These results are in agreement with those obtained by Martinez and colleagues (2003) using [¹¹C]Raclopride. In the **SB** subdivisions of the striatum, which has been the most commonly used method for the quantification of striatal dopamine release, the highest release was measured in the VST ([¹¹C]PHNO = 21.2 ± 6.93 %, [¹¹C]Raclopride = 14.1 ± 6.38 %) followed by putamen ([¹¹C]PHNO = 16.4 ± 4.42 %, [¹¹C]Raclopride = 11.7 ± 5.99 %) and the lowest in the caudate ([¹¹C]PHNO = 14.3 ± 6.84 %, [¹¹C]Raclopride = 7.68 ± 4.68 %). The data used here is the same data as in Shotbolt et al. (2011) who performed the analysis and quantification of dopamine release, in the **SB** subdivisions in the subject's native space. The quantification of dopamine release estimated with the two studies is comparable as no significant difference was detected. Quantification with [¹¹C]PHNO indicates that dopamine is released differentially (ANOVA test) in the structural-based subdivisions (**SBf** p = 0.009 and **SB** p = 0.03) but no differential dopamine release was detected for [¹¹C]Raclopride. For the [¹¹C]PHNO the limbic – executive pair showed a significant difference for the **SBf** method, whereas for the **SB** method the VST - caudate pair.

22
23
24
25
26
27
28
29
30
31
32
33
34
35
36
37
38
39
40
41
42
43
44
45
46
47
48
49
50
51
52
53
54
55 The %COV of dopamine release for each method and each subdivision was measured (Figure 5 B, D and table II) to assess the homogeneity of dopamine release. For the connectivity-based methods the average %COV was

1
2
3 23.48% for [¹¹C]PHNO and 48.11% for [¹¹C]Raclopride. A higher average %COV was measured in the **SBf** in
4
5 comparison with the connectivity-based subdivisions. In particular, the average %COV for [¹¹C]PHNO was
6
7 33.3% and for [¹¹C]Raclopride 52.2%. For the **SB** the average %COV is 35.9% for [¹¹C]PHNO and 52.5% for
8
9 [¹¹C]Raclopride. As we progress from the structural subdivisions to more sophisticated connectivity-based
10
11 subdivisions, dopamine release becomes more homogenous (low %COV) (figure 5). To assess these
12
13 differences the non-parametric Mann-Whitney test was implemented to compare the homogeneity of
14
15 dopamine release in the **CB** (limbic, executive, rostral-motor, caudal-motor, parietal) versus the structural-
16
17 based ROIs (caudate, putamen, VST (limbic), caudate/pre-commissural putamen (executive) and post-
18
19 commissural putamen (sensorimotor)). The results show that homogeneity of dopamine release was
20
21 significantly higher in the **CB** ROIs for both ligands ([¹¹C]PHNO (p=0.05) and [¹¹C]Raclopride (p=0.03)). However,
22
23 our concern was that these significant differences might be driven by the fact that some of the **CB** ROIs are
24
25 small in size, which might lead to lower %COVs. There was no correlation between the %COV and the size for
26
27 each ROI (p=0.3) (supplemental material figure 7).

28
29 According to Haber and colleagues (Haber *et al.* 2006) limbic–executive overlapping areas mediate incentive
30
31 learning and these areas might be particularly sensitive to dopamine modulation. The release of dopamine
32
33 within the overlapping ROIs was quantified with [¹¹C]PHNO only, as it has been shown previously to provide a
34
35 greater signal-to-noise ration than [¹¹C]Raclopride in studies of acute fluctuations in synaptic dopamine in the
36
37 human striatum (Shotbolt *et al.* 2011). The release of dopamine as measured by %BP_{ND} changes in the
38
39 overlapping limbic – executive area was 18.2 ± 5.39 % (limbic alone = 19.61 ± 6.78 %, and executive alone =
40
41 14.13 ± 4.12 %, supplemental material, Table IV, using the **CBo** method (1% threshold)). The results show that
42
43 d-amphetamine does not provoke a higher dopamine release in the overlapping area. In other overlapping
44
45 areas dopamine release (as measured by %BP_{ND} change) was: executive – rostral-motor = 14.7 ± 4.15 %;
46
47 executive – caudal-motor = 16.2 ± 5.05 %; and rostral-motor – caudal-motor = 16.0 ± 4.78 %, which also reflect
48
49 dopamine release similar to the independent areas they form part of (supplemental material, Table IV).

50
51 For comparison, dopamine release and its %COV were estimated within the connectivity-based functional ROIs
52
53 at thresholds of 1% and 10% and results are presented in the supplementary material (Table IV).
54
55
56
57
58
59
60

Discussions

Connectivity-based functional subdivision of the striatum

Our findings show bilaterally symmetric and topographically consistent projections of the cortical targets to the striatum, which are organised into discrete and overlapping networks. The spatial consistency of the connectivity-based subdivisions is reflected quantitatively and qualitatively by the DICE coefficients (supplemental material) and the consistency of the functional classifications across subjects respectively (figure 3B).

As Parent (Parent and Hazrati 1995) reports and shown in this study virtually all cortical areas contribute, at varying degrees, to the cortical-striatal projections. Consequently, the projections from all cortical lobes to striatum were considered for a comprehensive examination of the functional organisation of the striatum. The frontal lobe connections are dominant contributing $82\pm 7\%$ of the total striatal volume and are the main source that influences the functional organisation of the striatum. A detailed anatomical subdivision of the frontal lobe was performed, with each subdivision associated with a particular function, and the projections from each subdivision were estimated. As with non-human primate data (Haber *et al.* 2006) the ventral-medial prefrontal and orbital cortices connect to the anterior ventral caudate and putamen, the nucleus accumbens and also the ventral post-commissural putamen, which in primates also receives projecting fibers from the amygdala (Fudge *et al.* 2002). A discrepancy we observed between our results and the primate tracing studies, is that the limbic projections do not extend to the medial wall of the pre-commissural caudate (Haber *et al.* 2006). This might be due to the fact that this projection is very thin and with the current DWI resolution it has not been possible to recover it. In addition, we explored the projections of the cingulate cortex (areas 32/24) to understand if in humans this contributes to the medial limbic territory but such connections were not detected. The limbic volume contributes to $20\pm 7\%$ of the total striatal volume, which corresponds well with primate limbic volumetric estimates of 22% from tracing studies (Haber *et al.* 2006). Amygdala and hippocampus complex was excluded from the limbic target as their connectivity pattern was not consistent with previous human DWI studies (Cohen *et al.* 2009) and non-human primate tracing studies. As expected, projections from these structures were found in the VST area and the ventral post-commissural putamen. However, in most of our subjects strong connections were observed in the lateral anterior caudate, next to the

1
2
3 internal capsule and also in the lateral putamen parallel to the external capsule. Although termination and
4 exclusion masks were used to investigate further these projections, the results were inconclusive and these
5 structures were excluded from the limbic target.
6
7

8
9 The executive projections occupy large portion of the striatum and this finding contradicts the concept that
10 striatum is primarily a motor functional region. Projections from this target were found in rostral striatum and
11 extended post-commissurally (figures 3, 4). In our data, the probability of connections for tracts originating
12 from the executive target showed a degree of variability in the anterior caudate (Figure 3). These results are in
13 agreement with those of Lehericy and colleagues (Lehericy *et al.* 2004) who reported tracking variability across
14 subjects in the anterior striatum. Rostral-motor projections occupy the dorsal tier of rostral striatum and
15 extend to dorsal putamen caudal to the anterior-commissure. Our findings are consistent with those of non-
16 human tracing studies (Haber 2003) and other DWI studies in humans (Draganski *et al.* 2008). The caudal-
17 motor projections reside in the post-commissural striatum. These projections overlap with the rostral-motor
18 projections caudal to the anterior-commissure and extend further posteriorly. The pattern of cortical
19 projections to the striatum supports the theory of elongated rostral-caudal domains (Selemon and Goldman-
20 Rakic 1985).
21
22
23
24
25
26
27
28
29
30
31
32
33

34 For the rest of the brain, a coarse anatomical approach was followed, by estimating the projections from the
35 entire lobe. Areas where parietal lobe projections dominate occupy 11 ± 5 %, the second biggest cortical-striatal
36 connections, and reside mainly in the posterior striatum. In eight out of twelve subjects we observed small
37 patches of parietal projections in the anterior striatum (figure 3B) mainly in the central caudate, a finding that
38 is consistent with primate studies (Cavada and Goldman-Rakic 1989). Parietal lobe is a functionally
39 heterogeneous structure that consists of executive, visual, somatosensory and limbic sub-regions. At first we
40 considered parcellating the parietal lobe into anatomical subdivisions that would represent the four functions.
41 Nevertheless taking into consideration evidence from tracing studies that: a) the visual cortex contributes the
42 least from all the cortical regions (Kemp and Powell 1970; Parent and Hazrati 1995); and b) the limbic areas of
43 the parietal lobe are connected with visual and somatosensory areas (Cavada and Goldman-Rakic 1989), we
44 decided that it is preferable to subdivide the parietal lobe only into the somatosensory area (SS) and posterior
45 parietal (PP) area as described elsewhere (Behrens, Johansen-Berg, *et al.* 2003; Bohanna *et al.* 2011). However,
46 the projections from these two areas, SS and PP, show an extensive overlap, an observation confirmed by
47
48
49
50
51
52
53
54
55
56
57
58
59
60

1
2
3 Bohanna et al. (2011) and Cavada et al. (1991) that did not justify the subdivision of the parietal into SS and PP.
4
5 Therefore, considering parietal lobe as one entity was the most reliable choice.
6

7
8 Temporal and occipital lobes have limited connections with the striatum. Temporal projections in non-human
9
10 primates have been reported in the ventral-medial anterior caudate (Selemon and Goldman-Rakic 1985) and
11
12 the tail of the caudate (Van Hoesen et al. 1981). However, we did not observe projections to the tail of the
13
14 caudate. This discrepancy might be due to the fact that the caudate ROI did not include the whole tail of the
15
16 structure as the small size of the tail did not allow reliable tracing for all slices. Our cortical-striatal projections
17
18 are in agreement with those reported by Bohanna et al. (2011) with the exception that we did not observe any
19
20 projections from the occipital lobe to the caudate.
21

22
23 Accumulating evidence (Haber *et al.* 2006; Draganski *et al.* 2008) supports the concept of distinctive and
24
25 overlapping networks in the striatum, which form the basis for reward-based learning and goal-directed
26
27 behaviours. Our findings support the existence of overlapping projections throughout the human striatum,
28
29 engaging striatum in integrating information between functions, via overlapping networks. Our results indicate
30
31 that the executive area overlaps with all the other functional areas (limbic, rostral-motor, caudal-motor). This
32
33 suggests executive involvement in both motor and limbic functions; in other words, it points to a role for the
34
35 striatum in orchestrating the top-down component of action planning and selection.
36

37 **Release of dopamine**

38
39 D-amphetamine-induced reduction of the BP_{ND} has been well validated as a measure of change in synaptic
40
41 endogenous dopamine (Laruelle 2000). To date, both agonist and antagonist ligands have been used to
42
43 explore dopamine release in striatal subdivisions, which have been defined based on structural criteria
44
45 (Martinez *et al.* 2003; Shotbolt *et al.* 2011). Here, the agonist ($[^{11}C]$ PHNO) and antagonist ($[^{11}C]$ Raclopride)
46
47 ligands have been used to quantify dopamine release within the functional and structural subdivision of the
48
49 striatum.
50

51
52 In the connectivity-based functional subdivisions of the striatum the highest release of dopamine was
53
54 measured in the limbic, followed by the parietal, motor and executive functions. This pattern was repeated for
55
56 both ligands and was consistent across the different approaches taken to define the functional subdivisions
57
58 (**CB**, **CBo**). A statistical comparison for each functional area separately showed that the release of dopamine is
59
60

1
2
3 not affected by the connectivity-based ROIs employed to measure it, which indicates that connectivity-based
4 subdivision of the striatum is a robust method for the quantification of the PET signal (see also supplemental
5 material). As mentioned, the cortical-striatal projections are organised into discrete and overlapping networks.
6
7 The advantage of using methods that define the connectivity based ROIs by applying a lower threshold to the
8 connection maps (**CBo**) over the method that defines **CB** is that it includes voxels that are exclusively
9 connected (discrete network) to a cortical target as well as voxels that concurrently connect to other targets
10 (overlapping networks). The differences observed between the [¹¹C]Raclopride and [¹¹C]PHNO ligands with
11 regard to the pairs that exhibit significant difference, is consistent with the lower sensitivity of [¹¹C]Raclopride
12 in detecting dopamine release (Narendran *et al.* 2004; Shotbolt *et al.* 2012) and the smaller sample size for
13 [¹¹C]Raclopride in this study (sample size: nine subjects compared to twelve for [¹¹C]PHNO).
14
15
16
17
18
19
20
21
22

23 The **Sbf** method, like the **CB** method, assigns a sole function to every voxel. The **Sbf** method has detected
24 significant differences between the limbic and executive regions, whereas the significant differences between
25 the limbic and sensorimotor areas found with the **CB** were not preserved. This indicates that estimation of
26 dopamine release across the caudate/pre-commissural putamen complex and across the post-commissural
27 putamen and assigning an executive and sensorimotor function respectively as proposed by Martinez *et al.*
28 (Martinez *et al.* 2003), is not optimal. Nevertheless, the delineation of VST using the anatomical landmarks
29 described in Tziortzi *et al.* (Tziortzi, Searle, Tzimopoulou, *et al.* 2011) and its assignment to the limbic function
30 is a good approximation as the dopamine release was similar with that obtained using the limbic **CB**. In
31 addition, the original guidelines that subdivide the striatum into ventral and dorsal (Drevets *et al.* 1999;
32 Mawlawi *et al.* 2001) also safeguard the functional interpretation of the scientific findings.
33
34
35
36
37
38
39
40
41
42
43

44 The homogeneity of dopamine release was assessed by calculating the %COV for each subdivision. Our data
45 demonstrate greater homogeneity of dopamine release in the connectivity-based functional ROIs as compared
46 to the structural subdivisions, which suggests that connectivity-based functional ROIs may be a better
47 representation of neurotransmission relevant sub-regions of the striatum. These data provide evidence that
48 there is an association between local dopamine release and cortical connectivity profiles of these regions.
49
50
51
52

53
54
55 The biggest change in the PET signal in our study was seen in the limbic striatum followed by the sensorimotor
56 and executive area. The magnitude of the PET signal change, following the administration of amphetamine, is
57
58
59
60

1
2
3 dependent on the amount of dopamine release, as well as the relative proportions of the D2R-like receptors in
4 each subdivision. Dopamine has a preferential affinity for the D3R, over the D2R^{high} followed by the D2R^{low}
5 therefore a given concentration of dopamine can be expected to occupy a greater proportion of D3R and
6 D2R^{high}. D3R and D2R^{high} are known to be abundant in the ventral striatum area where the limbic cortex
7 projects. This could potential explain the higher release of dopamine detected in the limbic region.
8 Nevertheless, the second highest level of dopamine release was measured in the sensorimotor striatal areas,
9 which are primarily located in the post-commissural putamen where the D3R contribution to the total
10 [¹¹C]PHNO signal is negligible (Tziortzi et al., 2011). A similar argument could be made for the ratio of
11 D2R^{high}:D2R^{low} being higher in the sensorimotor than the executive striatum, leading to greater changes in
12 signal following similar amounts of dopamine release. In order to test this, we compared the ratio of
13 [¹¹C]PHNO/[¹¹C]Raclopride BP_{ND} for the two regions (where D3 contribution in the two regions is negligible).
14 We found no evidence for a difference in the [¹¹C]PHNO/[¹¹C]Raclopride ratio between the two regions,
15 suggesting that differences in the relative regional proportions of D2R-like species are unlikely to be
16 responsible for the regional pattern of BP_{ND} change seen in our data. Thus the emerging hypothesis is that
17 amphetamine leads to a preferential release of dopamine in the limbic, followed by the sensorimotor and the
18 executive areas.

19
20
21
22
23
24
25
26
27
28
29
30
31
32
33
34
35 Dopamine release is elicited in all functional sub-territories of the striatum and this is consistent with the
36 diversity of physiological effects provoked after the administration of d-amphetamine, which includes
37 psychological and physical effects such as euphoria, psychomotor agitation, locomotor stimulation,
38 hyperactivity, increased libido, increased concentration. The universal striatal activation could be explained by
39 the anatomical arrangement of the cortico-striatal and striato-nigro-striatal pathways. The cortico-striatal
40 pathways are organized into individual and overlapping networks. In these overlapping areas the distinct
41 cortical loops converge and information is integrated and conveyed. The striato-nigro-striatal pathways form
42 an ascending spiral by which information from a striatal region is transferred to other areas of the striatum.
43 Specifically, Haber and colleagues postulate (Haber et al. 2000) that there is an interface between different
44 striatal regions via the midbrain dopamine cells, which creates a hierarchy of information flow. Thus, the
45 universal striatal activation could be due to a complex chain of events, beginning with motivation and
46
47
48
49
50
51
52
53
54
55
56
57
58
59
60

1
2
3 progressing to cognitive and motor activations, as explained by the feed-forward organisation of the striatal
4 network.
5

6
7 The results show that d-amphetamine does not provoke a higher dopamine release in the overlapping areas. It
8 is worth to note that d-amphetamine releases accumulated dopamine by reversing the dopamine transporter,
9 and is thus a good measure of overall dopamine system integrity. Physiological dopamine release is dependent
10 on the firing rate of dopamine neurons, controlled at several levels by feedback loops. Assessment of
11 physiological dopamine release in these overlapping striatal functional areas may be assessed via performance
12 of tasks that require multi-function engagement.
13
14
15
16
17
18

19
20 Several studies support a functional and structural decline of the human brain with age. For instance, a recent
21 study has demonstrated an age-related decline in white matter tract integrity (Voineskos et al. 2012) while a
22 PET study with [¹¹C]Raclopride has shown that there is an age-related loss of striatal D2R receptors (Rinne et
23 al. 1993). The current study aimed to recruit a narrow age range in order to minimize age related effects. If the
24 decline of the dopamine receptors and/or of the white matter tracts within a subject and across regions were
25 uniform then one would expect to affect to a similar degree the connectivity-derived regions and the
26 respective quantification of dopamine release. Nevertheless potential age related effects warrant a further
27 investigation. In this study, the prefrontal functional subdivisions were not derived from functional MRI
28 experiments but make use of the known areas of specific brain function, as determined from the human and
29 primate literature. We are not aware of how the spatial anatomical arrangements of these cortical areas are
30 affected in different neurological and psychiatric disorders. Therefore, if this methodology is to be applied to
31 diseased cohorts, the anatomical-functional cortical alterations should be considered. One limitation of this
32 study is that we did not apply any partial volume corrections (Aston et al. 2002) or resolution recovery
33 techniques (Shidahara et al. 2009; Shidahara et al. 2012). However, the study by Martinez and colleagues
34 (Martinez *et al.* 2003) has performed partial volume corrections and the results indicate that the differences in
35 the structural-based subdivisions with regard to dopamine release were greater, a finding that would only
36 benefit the methodology presented here.
37
38
39
40
41
42
43
44
45
46
47
48
49
50
51
52

53
54 In this study the connectivity-based functional subdivisions were applied to PET data for the quantification of
55 dopamine release. This methodology is not limited to the investigation of endogenous dopamine release and
56
57
58
59
60

1
2
3 can be of value in other studies. The improved regional discrimination of this method can be of value in group
4
5 comparisons, where the detection of specific functional differences are explored. The striatum of the human
6
7 brain has highly differentiated neurochemical architecture (Holt et al. 1997). This method can be used to study
8
9 the distribution of neurotransmitters in individual subjects, understand the neurochemical organisation or
10
11 differentiation and explore the complex interactions among neurochemical systems. Such capability may help
12
13 the development of novel therapeutic compounds and enhance the evaluation of novel radiopharmaceuticals.
14
15 This methodology may also provide a valuable tool for deep brain stimulation surgery planning and improve
16
17 the treatment of a variety of disorders such as pain, motor, obsessive-compulsive disorders, depression and
18
19 addiction.

20
21 In conclusion, our results demonstrate that DWI data can help identify functional subdivisions of the human
22
23 striatum and this is a robust method for the quantification of dopamine release. The functional organisation is
24
25 consistent among subjects and the human functional organisation has a pattern with distinctive and
26
27 overlapping networks as that obtained in primates. The use of connectivity-based functional subdivisions
28
29 improves the evaluation of regional differences in dopamine. In particular the homogeneity of dopamine
30
31 release was significantly higher within the connectivity-based functional subdivisions in comparison with the
32
33 structural subdivisions. The results support an association between local levels of dopamine release and
34
35 cortical connectivity fingerprints. D-amphetamine induced the highest dopamine release in the limbic followed
36
37 by the sensory, motor and executive areas. Our data suggest that the relative regional proportions of D2-like
38
39 receptors are unlikely to be responsible for this regional dopamine release pattern. It is envisaged that the
40
41 proposed multi-modal imaging approach will prove valuable in exploring striatal neurotransmission in healthy
42
43 humans and patients with psychosis, addiction and motor impairments and will help the development of novel
44
45 therapeutic drugs.

50 **Distribution of the connectivity-based functional striatal atlas**

51
52
53 The probabilistic atlas of the functional organisation of the striatum developed using this methodology is
54
55 available with the FSL software (<http://fsl.fmrib.ox.ac.uk/fsl/fslwiki/Atlases/striatumconn>). Two
56
57 versions of the atlas exist. The first version comprises of three (3) subdivisions (limbic, executive,
58
59

1
2
3 sensorimotor) whereas the second comprises of seven (7) subdivisions (limbic, executive, rostral-
4
5 motor, caudal-motor, parietal, occipital and temporal). Available are also the probabilistic maps of
6
7 each cortical – striatal projections, which allow voxels that are connected to more than one cortical
8
9 targets to be included (overlapping networks).
10

11 12 **Funding**

13
14
15 A. C. Tziortzi work was jointly supported by GlaxoSmithKline (GSK) and the Biotechnology and Biological
16
17 Sciences Research Council (BBSRC BB/G53035X/1). Additional support was received by National Institutes of
18
19 Health (MH045573, MH086400).
20
21

22
23 **Acknowledgments:** The authors would like to thank Dr. Anderson Winkler, Dr. Stamatios Sotiropoulos, Dr.
24
25 Ricarda Menke, Dr. Anca Popescu, Dr. Jesper Andersson, Professor Paul M. Matthews, Dr. Qi Guo, Dr. Yoko
26
27 Tanimura and Dr. Julia Lehman for useful discussions; Dr. Richard Hargreaves (Merck R&D) for the useful
28
29 discussion and provision of pre-clinical data on [¹¹C]PHNO.
30

31
32 **Conflict of interest:** G.S, E.A.R and R.N.G are employed by Imanova Limited, Burlington Danes Building,
33
34 Hammersmith Hospital, Du Cane Road, London, W12 0NN, UK.
35
36
37
38
39
40
41
42
43
44
45
46
47
48
49
50
51
52
53
54
55
56
57
58
59
60

Bibliography

- 1
2
3
4
5 Andersson JL, Skare S, Ashburner J. 2003. How to correct susceptibility distortions in spin-echo
6 echo-planar images: application to diffusion tensor imaging. *NeuroImage* 20:870-888.
7
8
9 Aston JA, Cunningham VJ, Asselin MC, Hammers A, Evans AC, Gunn RN. 2002. Positron emission
10 tomography partial volume correction: estimation and algorithms. *J Cereb Blood Flow Metab*
11 22:1019-1034.
12
13
14 Banerjee A, Prante O. 2012. Subtype-selective dopamine receptor radioligands for PET imaging:
15 current status and recent developments. *Curr Med Chem* 19:3957-3966.
16
17
18 Behrens TE, Johansen-Berg H, Woolrich MW, Smith SM, Wheeler-Kingshott CA, Boulby PA,
19 Barker GJ, Sillery EL, Sheehan K, Ciccarelli O, Thompson AJ, Brady JM, Matthews PM. 2003. Non-
20 invasive mapping of connections between human thalamus and cortex using diffusion imaging. *Nat*
21 *Neurosci* 6:750-757.
22
23
24 Behrens TEJ, Berg HJ, Jbabdi S, Rushworth MFS, Woolrich MW. 2007. Probabilistic diffusion
25 tractography with multiple fibre orientations: What can we gain? *NeuroImage* 34:144-155.
26
27
28 Behrens TEJ, Woolrich MW, Jenkinson M, Johansen-Berg H, Nunes RG, Clare S, Matthews PM,
29 Brady JM, Smith SM. 2003. Characterization and propagation of uncertainty in diffusion-weighted
30 MR imaging. *Magnetic Resonance in Medicine* 50:1077-1088.
31
32
33 Bohanna I, Georgiou-Karistianis N, Egan GF. 2011. Connectivity-based segmentation of the striatum
34 in Huntington's disease: vulnerability of motor pathways. *Neurobiol Dis* 42:475-481.
35
36
37 Boileau I, Payer D, Houle S, Behzadi A, Rusjan PM, Tong J, Wilkins D, Selby P, George TP, Zack
38 M, Furukawa Y, McCluskey T, Wilson AA, Kish SJ. 2012. Higher binding of the dopamine D3
39 receptor-preferring ligand [11C]-(+)-propyl-hexahydro-naphtho-oxazin in methamphetamine
40 polydrug users: a positron emission tomography study. *J Neurosci* 32:1353-1359.
41
42
43 Calzavara R, Maily P, Haber SN. 2007. Relationship between the corticostriatal terminals from areas
44 9 and 46, and those from area 8A, dorsal and rostral premotor cortex and area 24c: An anatomical
45 substrate for cognition to action. *Eur J Neurosci* 26:2005-2024.
46
47
48
49
50
51
52
53
54
55
56
57
58
59
60

1
2
3 Cavada C, Goldman-Rakic PS. 1989. Posterior parietal cortex in rhesus monkey: II. Evidence for
4 segregated corticocortical networks linking sensory and limbic areas with the frontal lobe. *J Comp*
5 *Neurol* 287:422-445.

6
7
8
9 Cavada C, Goldman-Rakic PS. 1991. Topographic segregation of corticostriatal projections from
10 posterior parietal subdivisions in the macaque monkey. *Neuroscience* 42:683-696.

11
12
13 Chang H, Fitzpatrick JM. 1992. A technique for accurate magnetic resonance imaging in the presence
14 of field inhomogeneities. *IEEE Trans Med Imaging* 11:319-329.

15
16
17 Chiavaras MM, Petrides M. 2000. Orbitofrontal sulci of the human and macaque monkey brain. *The*
18 *Journal of Comparative Neurology* 422:35-54.

19
20
21 Cohen MX, Schoene-Bake JC, Elger CE, Weber B. 2009. Connectivity-based segregation of the
22 human striatum predicts personality characteristics. *Nat Neurosci* 12:32-34.

23
24
25 Crosson PL, Johansen-Berg H, Behrens TE, Robson MD, Pinsk MA, Gross CG, Richter W, Richter
26 MC, Kastner S, Rushworth MF. 2005. Quantitative investigation of connections of the prefrontal
27 cortex in the human and macaque using probabilistic diffusion tractography. *J Neurosci* 25:8854-
28 8866.

29
30
31 Draganski B, Kherif F, Klöppel S, Cook PA, Alexander DC, Parker GJM, Deichmann R, Ashburner J,
32 Frackowiak RSJ. 2008. Evidence for segregated and integrative connectivity patterns in the human
33 basal ganglia. *J Neurosci* 28:7143-7152.

34
35
36 Drevets WC, Price JC, Kupfer DJ, Kinahan PE, Lopresti B, Holt D, Mathis C. 1999. PET measures of
37 amphetamine-induced dopamine release in ventral versus dorsal striatum. *Neuropsychopharmacology*
38 21:694-709.

39
40
41 Egerton A, Mehta MA, Montgomery AJ, Lappin JM, Howes OD, Reeves SJ, Cunningham VJ, Grasby
42 PM. 2009. The dopaminergic basis of human behaviors: A review of molecular imaging studies.
43 *Neurosci Biobehav Rev* 33:1109-1132.

44
45
46 Fudge JL, Kunishio K, Walsh P, Richard C, Haber SN. 2002. Amygdaloid projections to
47 ventromedial striatal subterritories in the primate. *Neuroscience* 110:257-275.

- 1
2
3 Gallezot JD, Beaver JD, Gunn RN, Nabulsi N, Weinzimmer D, Singhal T, Slifstein M, Fowles K,
4
5 Ding YS, Huang Y, Laruelle M, Carson RE, Rabiner EA. 2012. Affinity and selectivity of [(1)(1)C]-
6
7 (+)-PHNO for the D3 and D2 receptors in the rhesus monkey brain in vivo. *Synapse* 66:489-500.
8
9 Gunn RN, Lammertsma AA, Hume SP, Cunningham VJ. 1997. Parametric imaging of ligand-receptor
10
11 binding in PET using a simplified reference region model. *NeuroImage* 6:279-2787.
12
13 Gurevich EV, Joyce JN. 1999. Distribution of Dopamine D3 receptor expressing neurons in the
14
15 human forebrain comparison with D2 receptor expressing neurons. *Neuropsychopharmacology* 20:60
16
17 - 80.
18
19 Haber SN. 2003. The primate basal ganglia: parallel and integrative networks. *J Chem Neuroanat*
20
21 26:317-330.
22
23 Haber SN, Fudge JL, McFarland NR. 2000. Striatonigrostriatal pathways in primates form an
24
25 ascending spiral from the shell to the dorsolateral striatum. *J Neurosci* 20:2369-2382.
26
27 Haber SN, Kim KS, Maily P, Calzavara R. 2006. Reward-related cortical inputs define a large striatal
28
29 region in primates that interface with associative cortical connections, providing a substrate for
30
31 incentive-based learning. *J Neurosci* 26:8368-8376.
32
33 Holt DJ, Graybiel AM, Saper CB. 1997. Neurochemical architecture of the human striatum. *J Comp*
34
35 *Neurol* 384:1-25.
36
37 Jenkinson M, Bannister P, Brady M, Smith S. 2002. Improved optimization for the robust and
38
39 accurate linear registration and motion correction of brain images. *NeuroImage* 17:825-841.
40
41 Johansen-Berg H, Behrens TE, Sillery E, Ciccarelli O, Thompson AJ, Smith SM, Matthews PM.
42
43 2005. Functional-anatomical validation and individual variation of diffusion tractography-based
44
45 segmentation of the human thalamus. *Cereb Cortex* 15:31-39.
46
47 Kegeles LS, Abi-Dargham A, Frankle WG, Gil R, Cooper TB, Slifstein M, Hwang DR, Huang Y,
48
49 Haber SN, Laruelle M. 2010. Increased synaptic dopamine function in associative regions of the
50
51 striatum in schizophrenia. *Arch Gen Psychiatry* 67:231-239.
52
53 Kemp JM, Powell TP. 1970. The cortico-striate projection in the monkey. *Brain* 93:525-546.
54
55 Kringelbach ML, Rolls ET. 2004. The functional neuroanatomy of the human orbitofrontal cortex:
56
57 evidence from neuroimaging and neuropsychology. *Progress in Neurobiology* 72:341-372.
58
59
60

- 1
2
3 Lammertsma AA, Hume SP. 1996. Simplified Reference Tissue Model for PET Receptor Studies.
4
5 NeuroImage 4:153-158.
6
7 Laruelle M. 2000. Imaging synaptic neurotransmission with in vivo binding competition techniques:
8
9 A critical review. J Cereb Blood Flow Metab 20:423-451.
10
11 Laruelle M. 2012. Measuring dopamine synaptic transmission with molecular imaging and
12
13 pharmacological challenges: The state of the art molecular imaging in the clinical neurosciences. In:
14
15 Gründer G, editor. Humana Press p 163-203.
16
17 Leh SE, Ptito A, Chakravarty MM, Strafella AP. 2007. Fronto-striatal connections in the human brain:
18
19 a probabilistic diffusion tractography study. Neurosci Lett 419:113-118.
20
21 Lehericy S, Ducros M, Van De Moortele P-F, Francois C, Thivard L, Poupon C, Swindale N, Ugurbil
22
23 K, Kim D-S. 2004. Diffusion tensor fiber tracking shows distinct corticostriatal circuits in humans.
24
25 Ann Neurol 55:522-529.
26
27 Martinez D, Slifstein M, Broft A, Mawlawi O, Hwang D-R, Huang Y, Cooper T, Kegeles L, Zarahn
28
29 E, Abi-Dargham A, Haber SN, Laruelle M. 2003. Imaging human mesolimbic dopamine transmission
30
31 with positron emission tomography. part II: Amphetamine-induced dopamine release in the functional
32
33 subdivisions of the striatum. J Cereb Blood Flow Metab 23:285-300.
34
35 Mawlawi O, Martinez D, Slifstein M, Broft A, Chatterjee R, Hwang D-R, Huang Y, Simpson N, Ngo
36
37 K, Van Heertum R, Laruelle M. 2001. Imaging human mesolimbic dopamine transmission with
38
39 positron emission tomography: I. Accuracy and precision of D2 receptor parameter measurements in
40
41 ventral striatum. J Cereb Blood Flow Metab 21:1034-1057.
42
43 Mizrahi R, Addington J, Rusjan PM, Suridjan I, Ng A, Boileau I, Pruessner JC, Remington G, Houle
44
45 S, Wilson AA. 2012. Increased stress-induced dopamine release in psychosis. Biol Psychiatry 71:561-
46
47 567.
48
49 Mizrahi R, Agid O, Borlido C, Suridjan I, Rusjan P, Houle S, Remington G, Wilson AA, Kapur S.
50
51 2011. Effects of antipsychotics on D3 receptors: a clinical PET study in first episode antipsychotic
52
53 naive patients with schizophrenia using [11C]-(+)-PHNO. Schizophr Res 131:63-68.
54
55 Narendran R, Hwang DR, Slifstein M, Talbot PS, Erritzoe D, Huang Y, Cooper TB, Martinez D,
56
57 Kegeles LS, Abi-Dargham A, Laruelle M. 2004. In vivo vulnerability to competition by endogenous
58
59
60

1
2
3 dopamine: comparison of the D2 receptor agonist radiotracer (-)-N-[11C]propyl-norapomorphine
4 ([11C]NPA) with the D2 receptor antagonist radiotracer [11C]-raclopride. *Synapse* 52:188-208.

5
6 Parent A, Hazrati L-N. 1995. Functional anatomy of the basal ganglia. I. The cortico-basal ganglia-
7 thalamo-cortical loop. *Brain Research Reviews* 20:91-127.

8
9
10 Petrides M. 2005. Lateral prefrontal cortex: architectonic and functional organization. *Philosophical*
11 *Transactions of the Royal Society B: Biological Sciences* 360:781-795.

12
13 Rinne JO, Hietala J, Ruotsalainen U, Sako E, Laihin A, Nagren K, Lehtikoinen P, Oikonen V,
14
15 Syvalahti E. 1993. Decrease in human striatal dopamine D2 receptor density with age: a PET study
16 with [11C]raclopride. *J Cereb Blood Flow Metab* 13:310-314.

17
18
19 Selemon LD, Goldman-Rakic PS. 1985. Longitudinal topography and interdigitation of corticostriatal
20 projections in the rhesus monkey. *J Neurosci* 5:776-794.

21
22
23 Shapiro S, Wilk M. 1965. An analysis of variance test for normality (complete samples). *Biometrika*
24 52:591-611.

25
26
27 Shidahara M, Tsoumpas C, Hammers A, Boussion N, Visvikis D, Suhara T, Kanno I, Turkheimer FE.
28
29 2009. Functional and structural synergy for resolution recovery and partial volume correction in brain
30 PET. *Neuroimage* 44:340-348.

31
32
33 Shidahara M, Tsoumpas C, McGinnity CJ, Kato T, Tamura H, Hammers A, Watabe H, Turkheimer
34
35 FE. 2012. Wavelet-based resolution recovery using an anatomical prior provides quantitative recovery
36 for human population phantom PET [(11)C]raclopride data. *Phys Med Biol* 57:3107-3122.

37
38
39 Shotbolt P, Tziortzi AC, Searle GE, Colasanti A, van der Aart J, Abanades S, Plisson C, Miller SR,
40
41 Huiban M, Beaver JD, Gunn RN, Laruelle M, Rabiner EA. 2011. Within-subject comparison of
42 [(11)C]-(+)-PHNO and [(11)C]raclopride sensitivity to acute amphetamine challenge in healthy
43 humans. *J Cereb Blood Flow Metab*:127-136.

44
45
46 Shotbolt P, Tziortzi AC, Searle GE, Colasanti A, van der Aart J, Abanades S, Plisson C, Miller SR,
47
48 Huiban M, Beaver JD, Gunn RN, Laruelle M, Rabiner EA. 2012. Within-subject comparison of
49 [(11)C]-(+)-PHNO and [(11)C]raclopride sensitivity to acute amphetamine challenge in healthy
50 humans. *J Cereb Blood Flow Metab* 32:127-136.

- 1
2
3 Staley JK, Mash DC. 1996. Adaptive increase in D3 dopamine receptors in the brain reward circuits
4 of human cocaine fatalities. *J Neurosci* 16:6100-6106.
5
6
7 Suridjan I, Rusjan P, Addington J, Wilson AA, Houle S, Mizrahi R. 2012. Dopamine D2 and D3
8 binding in people at clinical high risk for schizophrenia, antipsychotic-naive patients and healthy
9 controls while performing a cognitive task. *J Psychiatry Neurosci* 37:110181.
10
11
12 Tziortzi AC, Searle G, Tsoumpas C, Long C, Shotbolt P, Rabiner E, Jenkinson M, Gunn R. 2011.
13 MR-DTI and PET multimodal imaging of dopamine release within subdivisions of basal ganglia.
14 *International Conference on Image Optimisation in Nuclear Medicine (Optimn)* 317.
15
16
17 Tziortzi AC, Searle GE, Tzimopoulou S, Salinas C, Beaver JD, Jenkinson M, Laruelle M, Rabiner
18 EA, Gunn RN. 2011. Imaging dopamine receptors in humans with [11C]-(+)-PHNO: dissection of D3
19 signal and anatomy. *NeuroImage* 54:264-277.
20
21
22 Van Hoesen GW, Yeterian EH, Lavizzo-Mourey R. 1981. Widespread corticostriate projections from
23 temporal cortex of the rhesus monkey. *J Comp Neurol* 199:205-219.
24
25
26 Voineskos AN, Rajji TK, Lobaugh NJ, Miranda D, Shenton ME, Kennedy JL, Pollock BG, Mulsant
27 BH. 2012. Age-related decline in white matter tract integrity and cognitive performance: a DTI
28 tractography and structural equation modeling study. *Neurobiol Aging* 33:21-34.
29
30
31 Wallis JD. 2007. Orbitofrontal Cortex and Its Contribution to Decision-Making. *Annual Review of*
32 *Neuroscience* 30:31-56.
33
34
35
36
37
38
39
40
41
42
43
44
45
46
47
48
49
50
51
52
53
54
55
56
57
58
59
60

Table I. Volume and percentage contribution to the total striatal volume of A) projections from each cortical target to the striatum after a threshold of 5% of the maximum connectivity value was applied (**CBo**, columns: 2-3); B) the volumes obtained after assigning each voxel to the cortical target with the highest connection probability (**CB**, columns: 4-6). Results are averaged between the left and right hemispheres.

Region/Function	CBo		CB		
	Volume (cm ³)	Contribution to total striatal volume (%)	Volume (cm ³)	Contribution to total striatal volume (%)	Contribution to frontal lobe associated volume (%)
Limbic	1.36 ± 0.49	11.68 ± 4.23 %	2.32 ± 0.79	20 ± 7 %	24 ± 9 %
Executive	3.04 ± 1.42	26.17 ± 12.37 %	5.73 ± 1.15	49 ± 9 %	60 ± 10 %
Rostral-motor	0.65 ± 0.40	5.64 ± 3.44 %	1.00 ± 0.53	9 ± 5 %	11 ± 6 %
Caudal-motor	0.65 ± 0.38	5.61 ± 3.37 %	0.45 ± 0.30	4 ± 3 %	5 ± 3 %
Parietal	2.50 ± 1.02	21.51 ± 8.93 %	1.29 ± 0.52	11 ± 5 %	-

Table II. Quantification of dopamine release within the connectivity-based functional subdivisions of the striatum for the [¹¹C]PHNO and [¹¹C]Raclopride ligands. Bottom row is the average %COV of dopamine release, averaged across functional subdivisions.

Ligand	[¹¹ C]PHNO		[¹¹ C]Raclopride	
	<i>CBo</i>	<i>CB</i>	<i>CBo</i>	<i>CB</i>
Limbic	21.03±7.33	20.75±5.94	13.50±4.30	14.01±5.40
Executive	13.89±3.26	13.87± 3.71	5.45±3.33	8.48±3.43
Rostral-motor	14.43±4.16	15.70±2.25	7.48±5.07	8.95±4.49
Caudal-motor	16.44±2.25	17.47±2.34	8.50±5.41	10.23±3.84
Parietal	16.78±4.39	18.11±3.68	11.78±4.67	11.28±5.49
Average %COV	24.40±7.78	20.69±6.95	52.83±15.98	43.07±5.93

1
2
3 Figure 1. A) Cortical subdivisions. Purple corresponds to frontal lobe, magenta to parietal, grey to temporal
4 lobe and orange to occipital lobe. Yellow corresponds to the executive, red to the limbic, green to the rostral-
5 motor, blue to the caudal-motor. B) Methods overview. To obtain the connectivity-based functional regions in
6 each subject a two-step procedure was applied: Phase I) the projections from the four brain lobes (frontal,
7 parietal, occipital, temporal) to the striatum were calculated and the striatal areas associated with each lobe
8 were established; Phase II) The frontal lobe was subdivided into four anatomical ROIs, each associated with a
9 particular functional specialisation (limbic, executive, rostral motor and caudal motor), and projections
10 between these anatomical ROIs and the striatal area associated with the frontal lobe was estimated
11
12
13
14
15
16
17
18

19 Figure 2. A) Group average projections, MNI space sagittal view, of the four cortical lobes to the striatum. Top
20 row left image, shows the four cortical lobe subdivisions: frontal lobe (purple), parietal (magenta), temporal
21 lobe (grey) and occipital lobe (orange). The first row shows the projections of each lobe to the caudate and
22 second row corresponds to projections in putamen. The beige colour corresponds to the striatal mask. B)
23 Areas within the striatum where the connections from each lobe prevail.
24
25
26
27
28
29

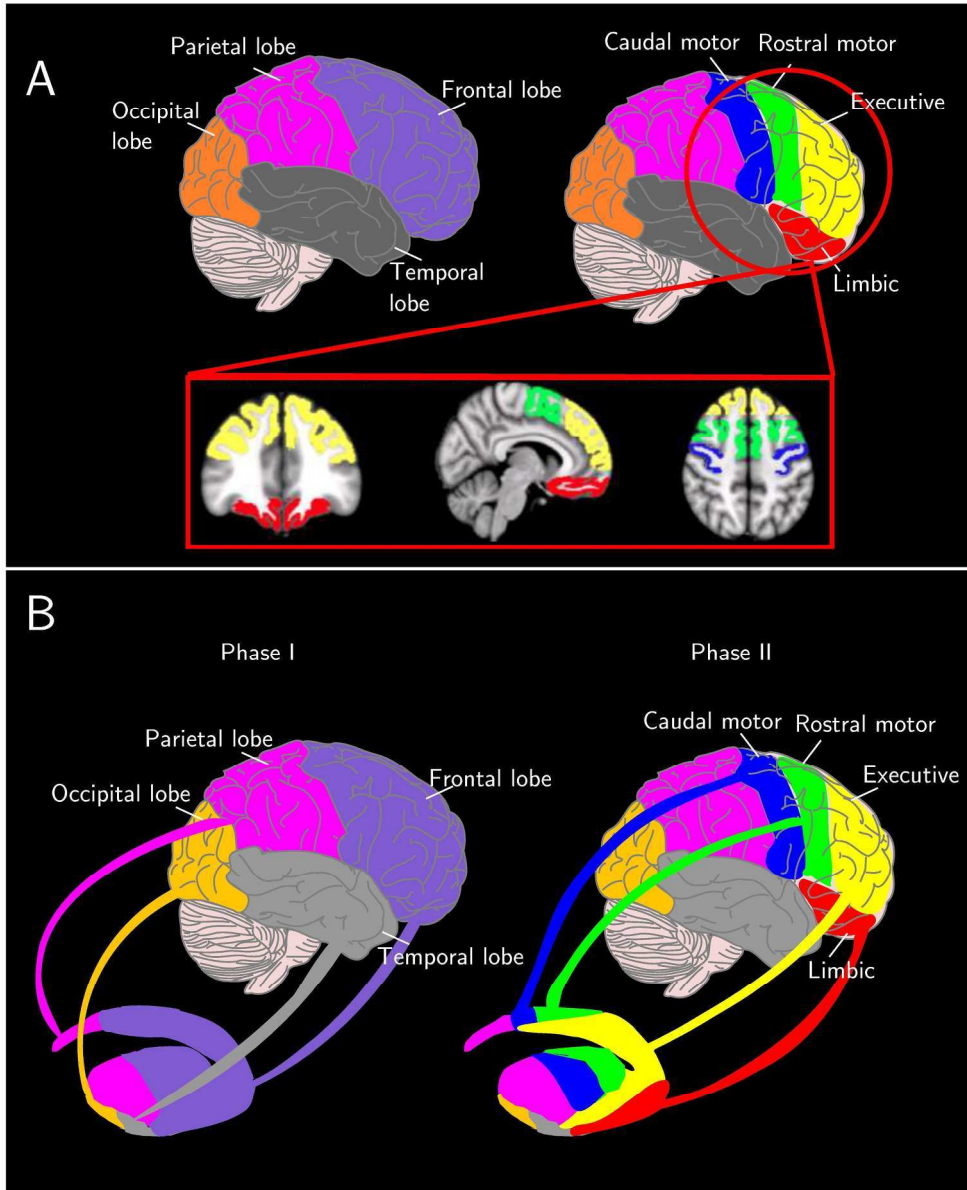
30 Figure 3. A) Group average projections from the four frontal lobe targets to the striatum. Each anatomical
31 target is associated to a specific function; limbic (first column), executive (second), rostral-motor (third) and
32 caudal-motor (fourth) functions. The rows correspond to different coronal planes (top row corresponds to
33 rostral striatum, bottom row to caudal striatum). A threshold of 50 samples was applied to the image in order
34 to discard noise and voxels with low connection probabilities. B) Individual functional subdivisions in four
35 randomly selected subjects (MNI space – coronal planes). Each column corresponds to a subject starting from
36 rostral (top row) to caudal (bottom row). To obtain the functional subdivision for each subject a two-step
37 procedure was applied. First the projections from the four brain lobes (frontal, parietal, occipital, temporal)
38 were calculated and each lobe's dominant area was established. Subsequently, the frontal lobe was subdivided
39 into four anatomical regions of interest, each associated with a specific function (limbic, executive, rostral-
40 motor and caudal-motor) and the projection of each target to the frontal lobe dominant area was estimated.
41 Each voxel was assigned to the target that gave the highest connection probability.
42
43
44
45
46
47
48
49
50
51
52

53 Figure 4. A) Group averaged functional subdivision of the striatum (MNI space – coronal planes). First column
54 corresponds to the pre-commissural and second column to post-commissural striatum. B) Overlapping
55
56
57
58
59
60

1
2
3 projections in the striatum (MNI space – coronal planes). The columns correspond to overlaps between: i)
4 limbic and executive (first column); ii) executive and rostral-motor (second column); iii) executive and caudal-
5 motor (third column); and iv) rostral-motor and caudal-motor (fourth column). A threshold of 50 samples was
6 applied to the projections and subsequently the overlapping areas were determined
7
8
9

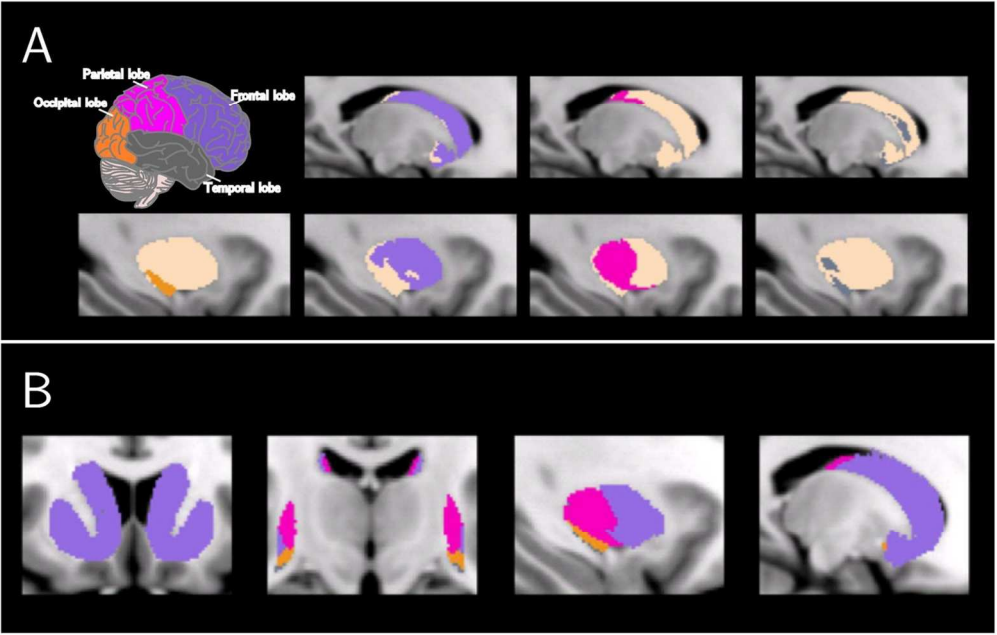
10
11 Figure 5. Dopamine release measured as the percentage change of the [^{11}C]PHNO BP_{ND} (column A) and
12 [^{11}C]Raclopride BP_{ND} (column C) within the exclusive connectivity-based functional regions of interest (CB, top
13 row), the structural-derived functional regions of interest (SBf, middle row) and the structural subdivisions of
14 the striatum (SB, bottom row). Columns B and D correspond to the dopamine release coefficient of variation
15 (%COV) for each region for the [^{11}C]PHNO and [^{11}C]Raclopride respectively. Abbreviations correspond to:
16 lim=limbic, exe=executive, rMt=rostral-motor, cMt=caudal-motor, par=parietal, sLim=structural-limbic,
17 sExe=structural-executive, sSm=structural-sensorimotor, VST=ventral striatum, CD=caudate, PU=putamen.
18
19
20
21
22
23
24
25
26
27
28
29
30
31
32
33
34
35
36
37
38
39
40
41
42
43
44
45
46
47
48
49
50
51
52
53
54
55
56
57
58
59
60

1
2
3
4
5
6
7
8
9
10
11
12
13
14
15
16
17
18
19
20
21
22
23
24
25
26
27
28
29
30
31
32
33
34
35
36
37
38
39
40
41
42
43
44
45
46
47
48
49
50
51
52
53
54
55
56
57
58
59
60



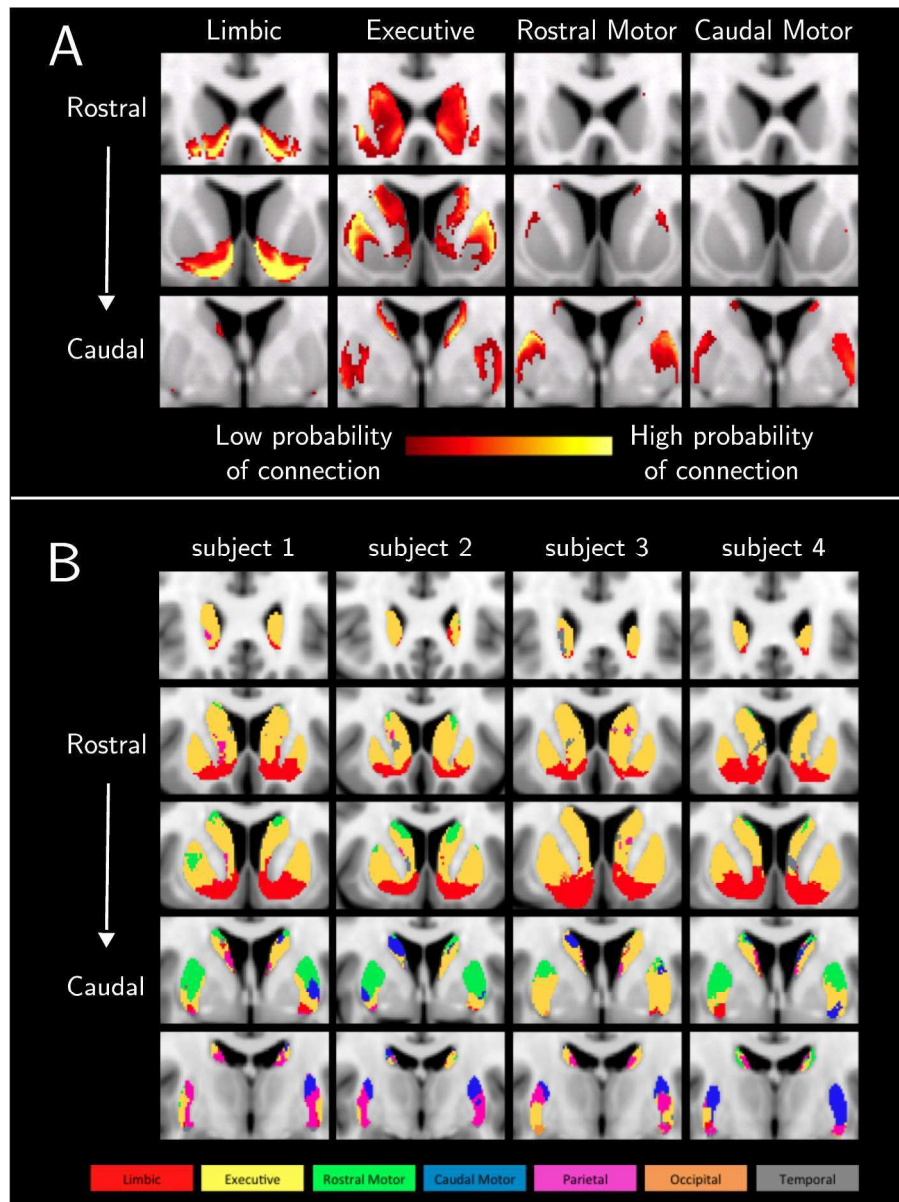
221x270mm (300 x 300 DPI)

1
2
3
4
5
6
7
8
9
10
11
12
13
14
15
16
17
18
19
20
21
22
23
24
25
26
27
28
29
30
31
32
33
34
35
36
37
38
39
40
41
42
43
44
45
46
47
48
49
50
51
52
53
54
55
56
57
58
59
60



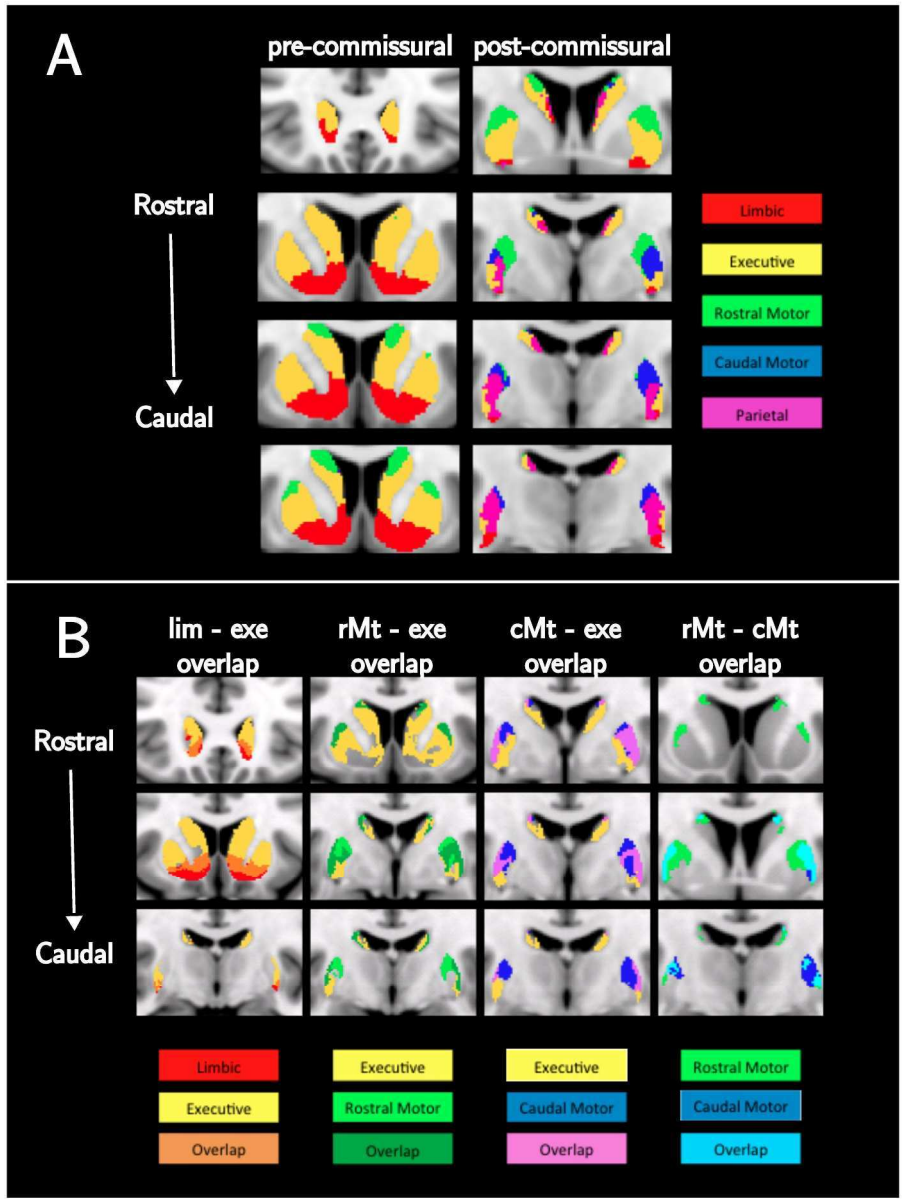
115x73mm (300 x 300 DPI)

Review

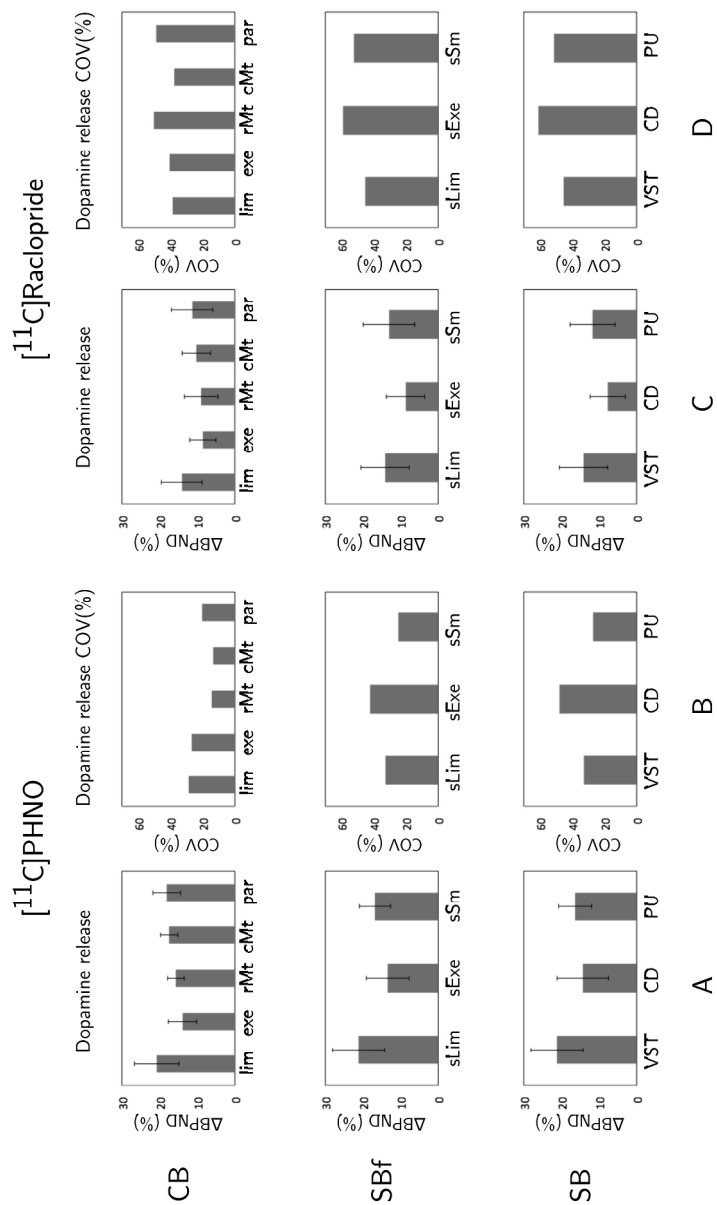


239x319mm (300 x 300 DPI)

1
2
3
4
5
6
7
8
9
10
11
12
13
14
15
16
17
18
19
20
21
22
23
24
25
26
27
28
29
30
31
32
33
34
35
36
37
38
39
40
41
42
43
44
45
46
47
48
49
50
51
52
53
54
55
56
57
58
59
60



240x321mm (300 x 300 DPI)



238x408mm (300 x 300 DPI)

1
2
3
4
5
6
7
8
9
10
11
12
13
14
15
16
17
18
19
20
21
22
23
24
25
26
27
28
29
30
31
32
33
34
35
36
37
38
39
40
41
42
43
44
45
46
47
48
49
50
51
52
53
54
55
56
57
58
59
60

Supplementary material

Connectivity-based functional analysis of dopamine release in the striatum using Diffusion Weighted MRI and Positron Emission Tomography

Inter-subject variability of the connectivity-based ROIs.

The DICE coefficient was estimated across subjects as the average overlap between a subject's **CB** with **CB** from each of the remaining 11 subjects in order to assess if the method and underlying connections were reproducible across subjects (individual subjects' scans were non-linearly registered to the MNI template). Dice coefficient was determined using equation 1:

$$DICE = 2 \cdot \frac{|ROI_1 \cap ROI_2|}{|ROI_1| + |ROI_2|} \cdot 100\% \quad (1)$$

where \cap is the intersection of the ROI volumes and ranges from 0 to 1. Thus, the DICE coefficient ranges from 0%, for ROIs with no overlap up to 100% for identical ROIs.

Dice coefficients for each **CB** were: limbic = 59.1 ± 12.4 %, executive = 63.2 ± 7.42 %, rostral-motor = 43.3 ± 12.0 %, caudal-motor = 29.5 ± 15.0 % and parietal = 39.8 ± 11.4 %. For the **CBo**: limbic = 52.29 ± 13.10 %, executive = 40.64 ± 10.79 %, rostral-motor = 36.62 ± 16.01 %, caudal-motor = 28.22 ± 15.44 % and parietal = 55.15 ± 10.13 %. Given that the DICE coefficient is affected by registration error and the size and geometry of the ROIs, the DICE values obtained for the limbic, parietal and executive striatum were high and satisfactory for the smaller rostral-motor and caudal-motor regions.

Connectivity-based ROIs with extra thresholds

Connectivity-based functional ROIs have been estimated with a threshold of 1% (**CBo_thr1**) and 10% (**CBo_thr10**) and the volumes can be seen in Table III. Figure 6 illustrates the impact of different thresholds on the topography and size of the cortical projections.

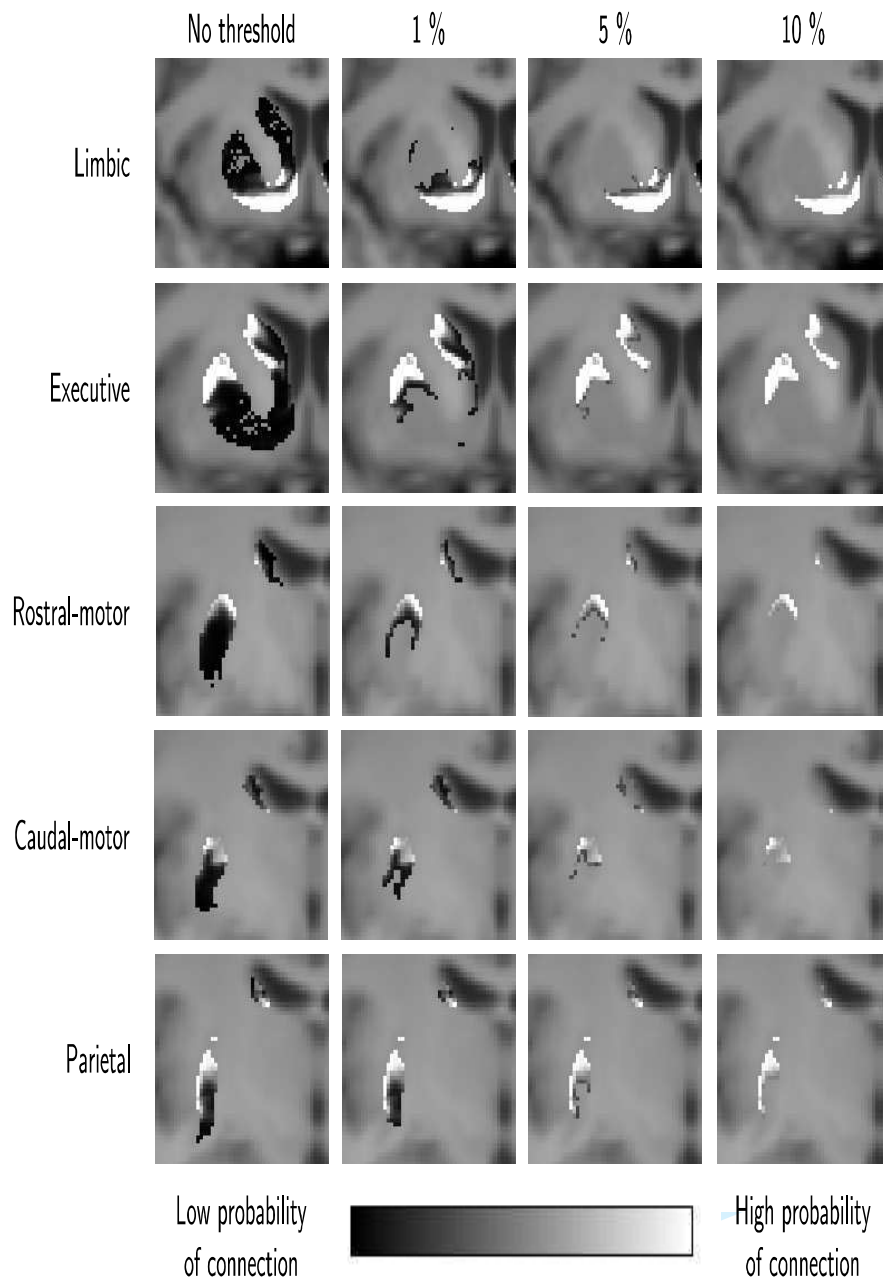


Figure 6. Effect of thresholds on the cortical-striatal connectivity maps in a representative subject. The first column shows the total projection from each target to the striatum. Subsequent columns show the connectivity maps after thresholded at 1%, 5% and 10% of the maximum connectivity value respectively.

1
2
3
4
5
6
7
8
9
10
11
12
13
14
15
16
17
18
19
20
21
22
23
24
25
26
27
28
29
30
31
32
33
34
35
36
37
38
39
40
41
42
43
44
45
46
47
48
49

Table III. Volume and percentage contribution to the total striatal volume of the cortical projection at thresholds of 1%, 5%, and 10% (*CBo* methods). *CB* is the volume and contribution to the striatal volume of exclusive connectivity-based ROIs (assignment of each voxel to the cortical target with the highest connection probability). Results are averaged between the left and right hemispheres.

Region/Function	<i>CBo_thr1</i>		<i>CBo</i>		<i>CBo_thr10</i>		<i>CB</i>	
	Volume (cm ³)	Contribution to total striatal volume (%)	Volume (cm ³)	Contribution to total striatal volume (%)	Volume (cm ³)	Contribution to total striatal volume (%)	Volume (cm ³)	Contribution to total striatal volume (%)
Limbic	2.42 ± 0.83	20.83 ± 7.17 %	1.36 ± 0.49	11.68 ± 4.23 %	1.03 ± 0.43	8.89 ± 3.69 %	2.32 ± 0.79	20 ± 7 %
Executive	5.86 ± 1.66	46.96 ± 14.18 %	3.04 ± 1.42	26.17 ± 12.37 %	1.97 ± 1.15	16.99 ± 10.08 %	5.73 ± 1.15	49 ± 9 %
Rostral-motor	1.67 ± 0.62	14.41 ± 5.48 %	0.65 ± 0.40	5.64 ± 3.44 %	0.36 ± 0.29	3.14 ± 2.53 %	1.00 ± 0.53	9 ± 5 %
Caudal-motor	1.67 ± 0.71	14.39 ± 6.23 %	0.65 ± 0.38	5.61 ± 3.37 %	0.33 ± 0.22	2.85 ± 1.94 %	0.45 ± 0.30	4 ± 3 %
Parietal	4.80 ± 1.56	41.30 ± 13.71 %	2.50 ± 1.02	21.51 ± 8.93 %	1.70 ± 0.71	14.63 ± 6.16 %	1.29 ± 0.52	11 ± 5 %

Dopamine release

Dopamine release and %COV of the dopamine release were estimated within the connectivity-based functional ROIs with thresholds at 1% (*CBo_thr1*) and 10% (*CBo_thr10*) and results are presented in Table IV. ANOVA test demonstrate that the difference in dopamine release across the connectivity-based methods is not significant. These particular thresholds were selected on the basis that these are the most commonly used thresholds in DWI studies (Behrens et al., 2003a; Croxson et al., 2005; Bohanna et al., 2011) with the further aim to assess the impact of thresholds and ROI size on the quantification of dopamine release.

The selection of an appropriate threshold is critical to detect regional differences in dopamine release. For [¹¹C]PHNO, which has higher sensitivity in detecting dopamine release than [¹¹C]Raclopride, all ROI methods except *CBo_thr1* have shown a significant difference in dopamine release between the limbic-executive and limbic-rostral motor pairs. The *CBo_thr1* approach applies the low threshold of 1% of the maximum connectivity value and this threshold might not be an appropriate selection to exclude noise and voxels with low connection probabilities.

Table IV. Quantification of dopamine release within the connectivity-based functional subdivisions of the striatum for the [¹¹C]PHNO and [¹¹C]Raclopride ligands.

Bottom row is the average %COV of dopamine release, averaged across functional subdivisions.

Threshold	¹¹ C]PHNO				¹¹ C]Raclopride			
	<i>CBo_thr1</i>	<i>CBo</i>	<i>CBo_thr10</i>	<i>CB</i>	<i>CBo_thr1</i>	<i>CBo</i>	<i>CBo_thr10</i>	<i>CB</i>
Limbic	19.61±6.78	21.03±7.33	21.15±7.50	20.75±5.94	13.98±6.58	13.50±4.30	13.71±4.07	14.01±5.40
Executive	14.13±4.12	13.89±3.26	13.61±3.16	13.87± 3.71	7.46±3.51	5.45±3.33	5.59±3.03	8.48±3.43
Rostral-motor	15.18±2.69	14.43±4.16	15.40±2.99	15.70±2.25	8.15±4.14	7.48±5.07	8.59±3.91	8.95±4.49
Caudal-motor	16.04±2.10	16.44±2.25	16.46±2.97	17.47±2.34	8.64±2.43	8.50±5.41	8.70±6.50	10.23±3.84
Parietal	16.32±4.29	16.78±4.39	16.87±4.59	18.11±3.68	10.49±6.32	11.78±4.67	11.43±5.18	11.28±5.49
Average %COV	24.16±8.68	24.40±7.78	24.69±7.01	20.69±6.95	46.66±11.65	52.83±15.98	49.89±16.45	43.07±5.93

ROI volume against dopamine release %COV

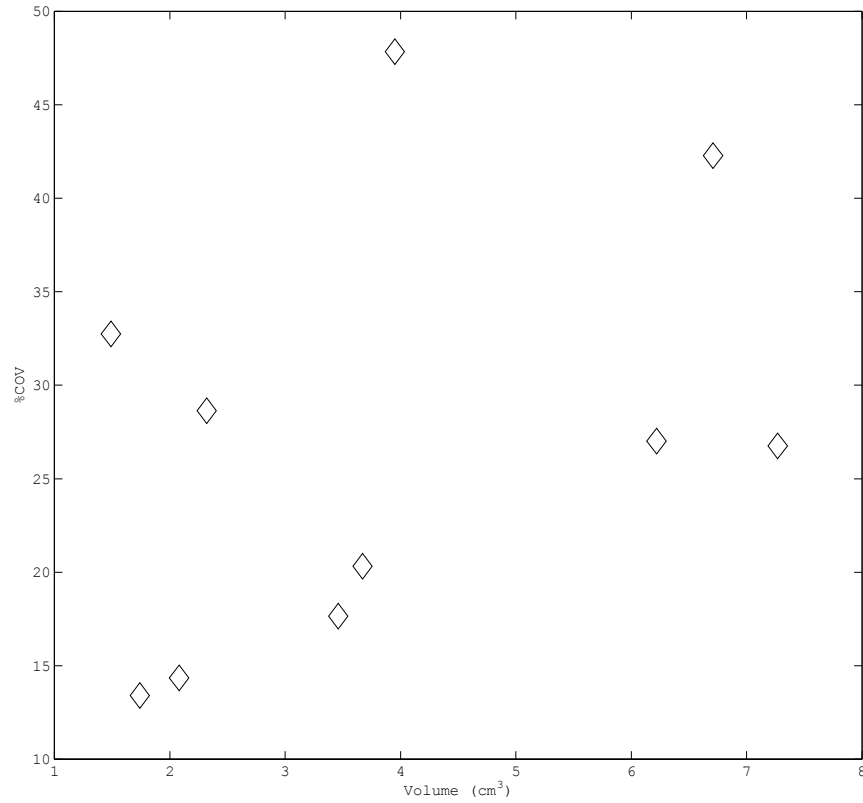


Figure 7. Volume of the region of interest against the %COV of dopamine release. No correlation was observed ($p=0.3$).